Available online at www.sciencedirect.com
ScienceDirect
Journal of African Earth Sciences 49 (2007) 153–178
Journal of African Earth Sciences
www.elsevier.com/locate/jafrearsci

The Temaguessine Fe-cordierite orbicular granite (Central Hoggar, Algeria): U–Pb SHRIMP age, petrology, origin and geodynamical consequences for the late Pan-African magmatism of the Tuareg shield

Nachida Abdallah [a], Jean-Paul Liégeois [b,*], Bert De Waele [c,1], Nassima Fezaa [d], Aziouz Ouabadi [a]

[a] *USTHB, Faculté des Sciences de la Terre, Aménagement du Territoire et de la Géographie, BP 32, El Alia, Bab Ezzouar, 16111 Alger, Algeria*
[b] *Isotope Geology, Royal Museum for Central Africa, B-3080 Tervuren, Belgium*
[c] *Tectonics Special Research Centre (TSRC), The University of Western Australia, School of Earth and Geographical Sciences, 35 Stirling Highway, WA 6009, Crawley, Australia*
[d] *ISMAL/Université d'Alger, Bois des Cars, Dély Ibrahim, Alger, Algeria*

Received 26 October 2006; received in revised form 20 August 2007; accepted 27 August 2007
Available online 7 September 2007

Abstract

The Temaguessine high-level subcircular pluton is intrusive into the LATEA metacraton (Central Hoggar) Eburnian (2 Ga) basement and in the Pan-African (615 Ma) granitic batholiths along a major NW–SE oriented major shear zone. It is dated here (SHRIMP U–Pb on zircon) at 582 ± 5 Ma. Composed of amphibole–biotite granite and biotite syenogranite, it comprises abundant enclaves: mafic magmatic enclaves, country-rock xenoliths and remarkable Fe-cordierite (#Fe = 0.87) orbicules. The orbicules have a core rich in cordierite (40%) and a leucocratic quartz–feldspar rim. They are interpreted as resulting from the incongruent melting of the meta-wacke xenoliths collapsed into the magma: the breakdown of the biotite + quartz assemblage produced the cordierite and a quartz–feldspar minimum melt that is expelled, forming the leucocratic rim. The orbicule generation occurred at $T < 850°$ and $P < 0.3$ GPa. The Fe-rich character of the cordierite resulted from the Fe-rich protolith (wacke with 4% Fe_2O_3 for 72% SiO_2). Strongly negative ε_{Nd} (−9.6 to −11.2), Nd T_{DM} model ages between 1.64 and 1.92 Ga, inherited zircons between 1.76 and 2.04 Ga and low to moderately high I_{Sr} (0.704–0.710) indicate a Rb-depleted lower continental crust source for the Temaguessine pluton; regional considerations impose however also the participation of asthenospheric material. The Temaguessine pluton, together with other high-level subcircular pluton, is considered as marking the end of the Pan-African magma generation in the LATEA metacraton, resulting from the linear delamination along mega-shear zones, allowing asthenospheric uprise and melting of the lower continental crust. This implies that the younger Taourirt granitic province (535–520 Ma) should be considered as a Cambrian intraplate anorogenic event and not as a very late Pan-African event.
© 2007 Elsevier Ltd. All rights reserved.

Keywords: Fe-cordierite; Orbicule; U–Pb zircon; Pan-African; Tuareg shield

1. Introduction

The Tuareg shield is made up of about 40% granitoids, among which most are post-collisional high-K calc-alkaline (Black et al., 1994; Fig. 1A). Most are of batholitic size, and intrude in the 620–580 Ma time interval along mega-shear zones linked to Pan-African post-collisional

* Corresponding author. Tel./fax: +32 2 6502252.
E-mail addresses: a_nachida@yahoo.fr (N. Abdallah), jean-paul.liegeois@africamuseum.be (J.-P. Liégeois), bdewaele@bgs.ac.uk (B. De Waele), fezaanassima@yahoo.fr (N. Fezaa), ouabadi@yahoo.fr (A. Ouabadi).
[1] Present address: British Geological Survey.

1464-343X/$ - see front matter © 2007 Elsevier Ltd. All rights reserved.
doi:10.1016/j.jafrearsci.2007.08.005

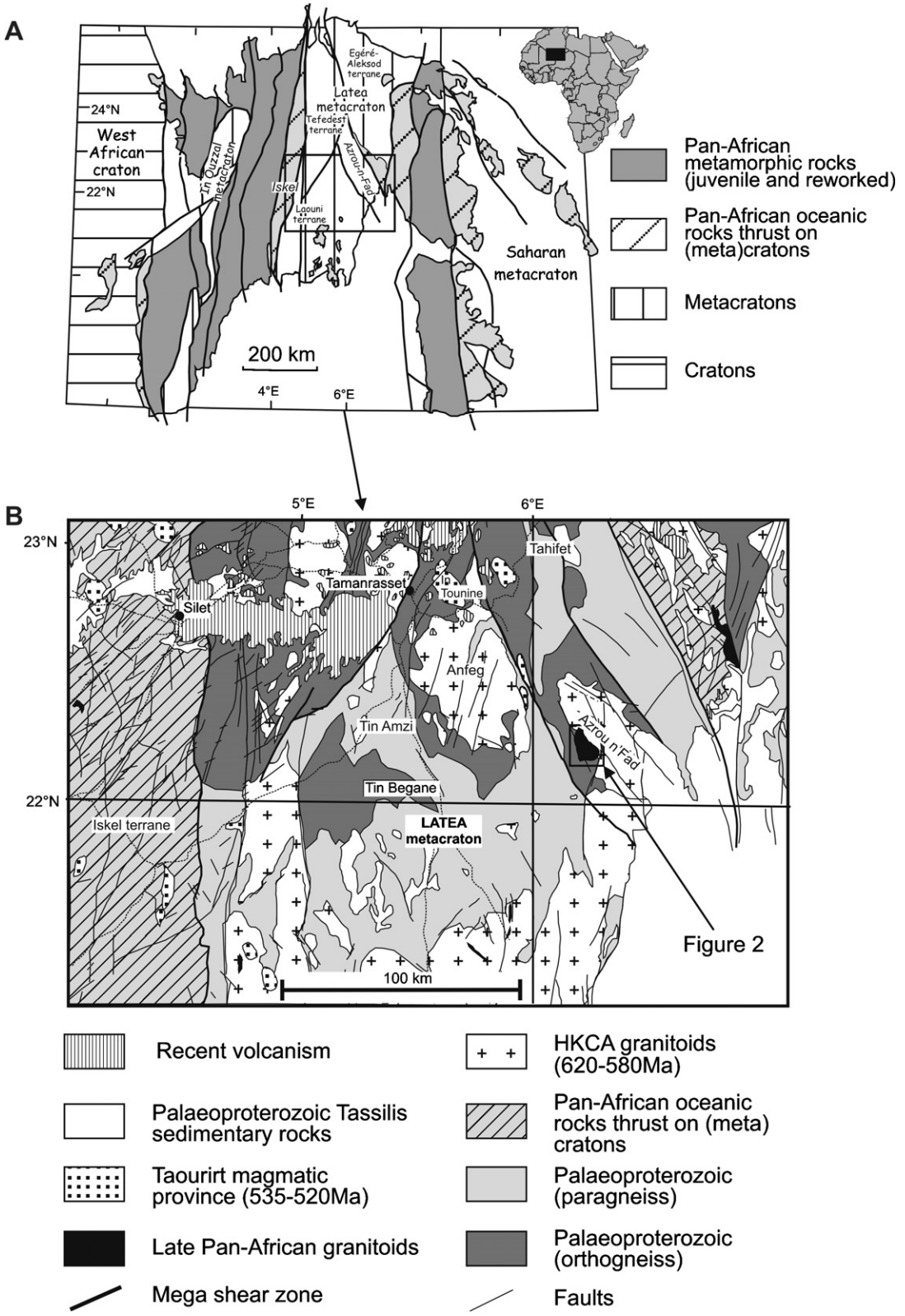

Fig. 1. (A) Tuareg shield terrane map (simplified from Black et al., 1994) and (B) geological map of the southern part of the LATEA metacraton (modified from Bertrand and Caby, 1977).

movements of the terranes constituting the Tuareg shield (Liégeois et al., 2003 and references therein). A series of later, higher level, circular plutons are known in the shield, mainly the Iforas alkaline–peralkaline ring-complexes (560–540 Ma; Liégeois et al., 1987), the Taourirt alkali-calcic province in Central Hoggar comprising some very small

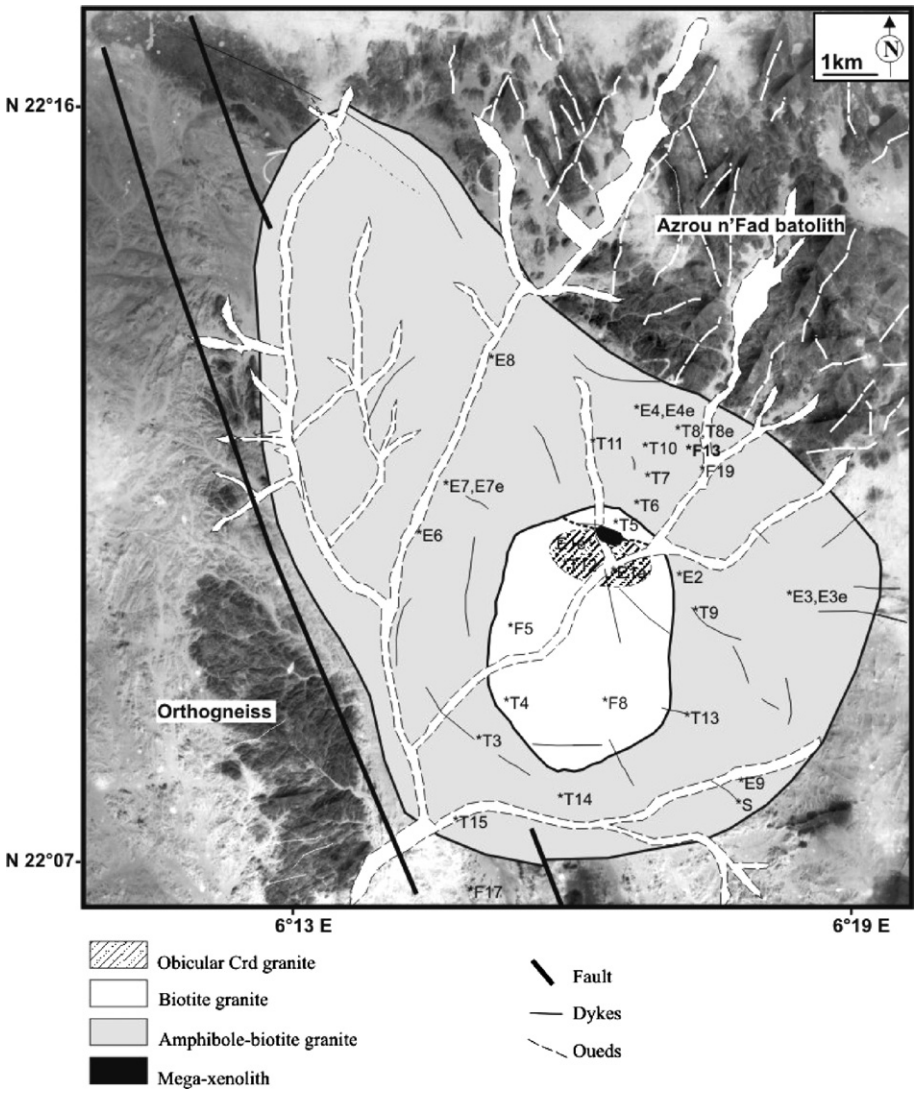

Fig. 2. Magmatic facies of the Temaguessine pluton showing sample locations.

topaz-bearing plutons or small topaz-bearing venues within larger plutons (535–525 Ma; Azzouni-Sekkal et al., 2003 and references therein) and some other isolated plutons, among which the Temaguessine pluton.

The Temaguessine granitic pluton is similar to the Taourirt plutons, in that it also has a high-level circular habit and has a highly potassic composition. It differs from the Taourirt suite in that it is isolated (Fig. 2), and in the presence of cordierite orbicules. Only three other occurrences of cordierite are known in the Tuareg shield granitoids, but none occur as cordierite orbicules. In Temaguessine, the nearly spherical cordierite orbicules are composed of a dark cordierite-bearing core and a light quartz–feldspar rim. The cordierite is iron-rich, which is not usual in granites (Clarke, 1995). No other aluminous mineral has been observed in this granite. In this paper, we present new geochronological, isotopic and geochemical data on this peculiar Fe-cordierite orbicule-bearing pluton, and will constrain its geodynamical position within the Tuareg Pan-African orogen, particularly with respect to the other late plutons. Additionally, we will propose a model for the genesis of cordierite orbicules within a potassic alkali-calcic granitic magma.

2. The Tuareg shield and the Azrou n'Fad terrane

The Tuareg shield in Central Sahara extends over more than 500 000 km^2 in Algeria, Mali and Niger (Fig. 1A). With a width of 1000 km, it is made of a series of terranes affected by the Pan-African orogeny (Black et al., 1994) and is located between the West African craton and the Saharan metacraton (Abdelsalam et al., 2002). The nature of these terranes is variable, from juvenile oceanic thrust terranes generated during the Neoproterozoic (Caby, 2003) to metacratonic Archaean–Palaeoproterozoic terranes only slightly affected by the Pan-African orogeny (e.g. In Ouzzal terrane; Ouzegane et al., 2003). In the centre of the shield, the composite Archaean/Palaeoproterozoic

LATEA microcontinent has been squeezed and dissected by shear zones along which large high-K calk-alkaline batholiths (Fig. 1B) have intruded (Liégeois et al., 2003). In LATEA, these batholiths are known in the 630–600 Ma age range (Bertrand et al., 1986; Liégeois et al., 2003). In the Tuareg shield, late high-level subcircular plutons with alkaline affinity are present: the large alkaline–peralkaline Iforas province (Liégeois and Black, 1987), the c. 555 Ma Tisselliline pluton (Egéré-Aleksod terrane; Liégeois et al., 2003), and the 535–525 Ma alkali-calcic Taourirt plutons (Boissonnas, 1973; Cheilletz et al., 1992; Paquette et al., 1998; Azzouni-Sekkal et al., 2003).

The Azrou n'Fad terrane is one of the terranes constituting the LATEA metacraton. It is thus made up of an Eburnian gneissic basement overthrust by Pan-African oceanic material including eclogites (Zetoutou et al., 2004) and intruded by Pan-African batholiths. It is bound by mega-shear zones except to the SE, where it is covered by the Tassilis Ordovician sandstones above an unconformity (Fig. 1B). It is narrow and elongated along NW–SE direction. As the other terranes of LATEA (acronym for Laouni, Azrou n'Fad, Tefedest and Egéré-Aleksod terranes; Fig. 1A), the Azrou n'Fad terrane is made of (1) a basement comprising orthogneisses whose U–Pb ages are around 2 Ga, and metasediments, both affected by amphibolite facies metamorphism (Bertrand et al., 1986); (2) Neoproterozoic amphibolite to eclogite-facies rocks thrust on this basement, that can be correlated with the Tin Begane region (Fig. 1B) where such units have been dated at c. 685 Ma (Liégeois et al., 2003); (3) large Pan-African high-K calc-alkaline batholiths comparable to the c. 615 Ma Anfeg batholith (Bertrand et al., 1986; Acef et al., 2003); and (4) late generally circular plutons emplaced at shallow level, among which the Temaguessine pluton.

3. The Temaguessine pluton

The Temaguessine pluton is located in the Tahifet area of the Azrou n'Fad terrane, 100 km to the SE of Tamanrasset (Fig. 1B). It is of particular interest as it contains cordierite orbicules. In the Tuareg shield, this mineral is only known from three other granitic plutons: cordierite has been described within the granitic mineral assemblage of the In Tounine pluton (Boissonnas, 1973 Fig. 1B) belonging to the Taourirt province (Azzouni-Sekkal et al., 2003) and in the Tihimatine late pluton within the In Ouzzal terrane to the west (Fezaa et al., 2005) and in gneissic xenoliths within the Tin Amzi batholith (Loumi, pers. comm., 2005).

The Temaguessine pluton (Fig. 2) intrudes: (1) to the south, the Eburnian basement composed of quartzite, migmatitic gneisses, biotite–garnet–sillimanite gneisses, and amphibolite–pyroxene marbles (Briedj, 1993; Zetoutou et al., 2004) forming a regional basin and dome structure (Briedj, 1993) similar to those of the Laouni terrane (Ouzegane et al., 2001; Peucat et al., 2003; Bendaoud et al., 2003; Derridj et al., 2003); (2) to the north (Fig. 3A), the large Azrou n'Fad granitic batholith (biotite–amphibole foliated granite), which is comparable to the Anfeg batholith, dated at 608 ± 7 Ma (U–Pb zircon, Bertrand et al., 1986; recalculated by Acef et al., 2003); the contact is sharp.

The oval-shaped Temaguessine pluton (11 × 8 km; Fig. 2) shows two facies: (1) amphibole–biotite granite with abundant dark and rare light microgranular magmatic enclaves and (2) biotite syenogranite with centimetre-size

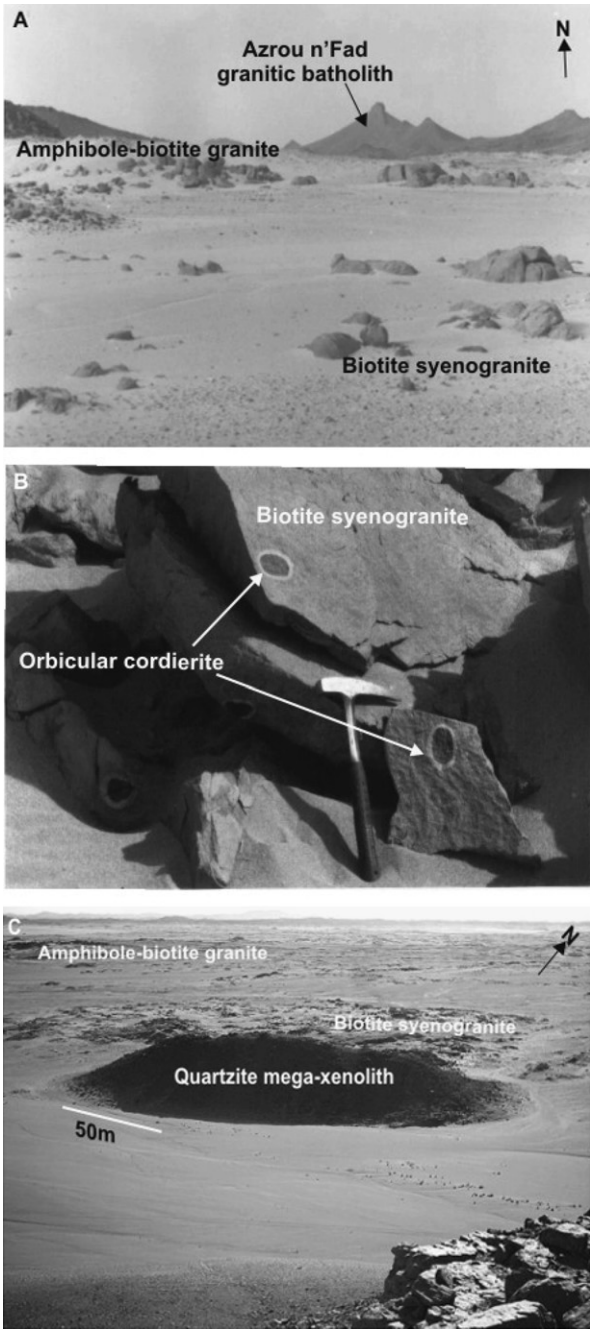

Fig. 3. (A) Typical outcrops of the Temaguessine granites with the Azrou n'Fad granitic batholith at the rear; (B) Cordierite orbicules in the biotite syenogranite; and (C) hectometre-size quartzite xenolith within the biotite syenogranite.

orbicules of cordierite (Fig. 3B). The orbicules are distributed over a surface of about 100×20 m along a large quartzite xenolith of the same length (Fig. 3C). The two granite facies are leucocratic: the normative quartz + feldspar are in the range 92–98% for the amphibole–biotite granite and 96–98% for the biotite syenogranite. The pluton is crosscut by abundant dykes, most being felsic and NW–SE oriented.

Mineral analyses are given in Table 1A (feldspars), 1B (amphibole), 1C (biotite), 1D (orthopyroxene) and 1E (cordierite).

3.1. The amphibole–biotite granite and the mafic microgranular enclaves (MME)

The amphibole–biotite granite represents the main facies of the Temaguessine pluton. It shows coarse- to fine-grained and often porphyritic textures. It is composed mainly of quartz, K–feldspar, plagioclase and biotite. Quartz is present as large crystals enclosing numerous feldspar and biotite crystals as well as oxide minerals. The K–feldspar is often of millimetre- to centimetre-size and has a composition of $0.94 < X_{orth} < 0.96$ (Table 1A). The amphibole has a composition of ferro-edenite and hastingsite (Fig. 4B; Table 1B) with Al_{tot} varying between 1.46 and 1.86. The plagioclase is an oligoclase (An_{27-29}). The biotite shows a ferriferous character ($0.80 < X_{Fe} < 0.54$), being close to the annite pole (Fig. 4A); the total Al varying between 2.30 and 2.35 (Table 1C). Zircon, allanite, titanite and rare oxides (mainly ilmenite) are the accessory minerals. Secondary chlorite and epidote can be found in the rock.

The Temaguessine amphibole–biotite granite comprises abundant light and dark microgranular enclaves. The light microgranular enclaves show the same mineralogy as the host granite with a finer grain size. The dark mafic microgranular enclaves show a doleritic texture and are composed of plagioclase (andesine-labrador: $0.44 < X_{An} < 0.64$), biotite ($0.04 < Al_t < 1.59$ and $0.59 < X_{Fe} < 0.68$) close to the annite pole as is the case for the amphibole–biotite granite (Fig. 4A), amphibole (edenite–hastingsite and Mg–hornblende ($0.18 < X_{Fe} < 0.63$) (Fig. 4B; Table 1D) and orthopyroxene (En: 58.46–65.31; Wo: 3.11–4.21; Fs: 30.92–37.64; Table 1D), which is an enstatite following Morimoto et al. (1989).

3.2. The biotite syenogranite and the orbicular cordierite

The biotite syenogranite is less abundant than the amphibole–biotite granite, and shows the same coarse- to fine-grained and often porphyritic textures. The plagioclase is less abundant than K–feldspar and is an oligoclase ($0.18 < X_{An} < 0.29$). Biotite is the only dark Fe–Mg mineral present in this rock, and forms small crystals. It is Fe-rich (X_{Fe} comprised between 0.82 and 0.70; Table 1C) and enriched in Al^{VI} (between 0.7 and 1; Fig. 4A), two characteristics indicating an important siderophyllite component (Fig. 4A). Accessory minerals include euhedral allanite, titanite, zircon and opaque crystals. Chlorite and epidote are the main alteration minerals. This facies does not contain MME but, by contrast, bears orbicular cordierite.

The orbicular cordierites are large spherical (10 cm in diameter or more) enclaves (Fig. 3B) composed of about half cordierite, the other half being composed of quartz, plagioclase (oligoclase An_{20}–An_{28}), biotite ghosts that have the same composition as the biotite from the biotite granite (Table 1C; Fig. 4A, C, D) and very rare K–feldspar. The cordierite crystals are generally limpid, euhedral, without any refractory inclusions and show irregular micro-cracks. Chemical analysis of this cordierite shows high FeO (14–17%) and low MgO (1.5–2.3%) contents with an X_{Fe} comprised between 0.79 and 0.80 (Table 1E). The cordierite orbicules are always surrounded by a quartz–feldspar corona, 2–3 cm thick. These observations indicate that the cordierite is not in equilibrium with the granitic liquid, and so it is not a primary phase of the magma.

Although the main chemical variation in the cordierite is the replacement of Mg by Fe^{+2}, iron-rich cordierite is rare in nature. We have compiled a series of cordierite Fe# present in magmatic rocks from the literature (Fig. 4E). Most of them have an Fe# (Fe/(Fe + Mn + Mg), molar proportion) between 0.4 and 0.5. The only cordierite richer in Fe than that of Temaguessine (Fe# = 0.87) is the cordierite of the Rubicon rhyolite (Fe# 0.98, Australia; Birch and Gleadow, 1974). There the Fe-cordierite is considered to result partly from the breakdown of biotite during anatexis leading to the crystallization of garnet, opx and Fe-cordierite, present in the rhyolite as residual phases. Cordierite is known within the LATEA gneissic assemblage in the Laouni area, to the west of Temaguessine (Guiraud et al., 1996). However, this cordierite is Mg-rich (Fe# = 0.29) precluding the hypothesis that the Temaguessine cordierite is directly coming from the country-rocks.

3.3. Dykes

Several dykes crosscut the Temaguessine pluton. They show a main NW–SE orientation. In the field, they correspond to dark rocks with blue-greenish colour to clear grey patina. They have a gabbroic composition: plagioclase, amphibole (brown and green hornblende) and pyroxenes. Their petrographical features are similar to those of the mafic microgranular enclaves.

4. Biotite typology of the Temaguessine pluton

The biotite of the two granitic facies of the Temaguessine pluton are well distinguished by the Al^{VI} content, close to 0 in the amphibole–biotite granite and in the enclaves and between 0.7 and 1 in the biotite granite and in the cordierite orbicule (Fig. 4A; siderophyllite component). As their Al^{IV} is comparable in all facies, this difference can be also observed in the Al_{tot} content of their biotite (Fig. 4C; Nachit et al., 1985): (1) the biotite from the biotite

Table 1A
Selected analyses of feldspars from the Temaguessine pluton

Faciès	Biotite granite						Amphibole–biotite granite								Enclaves											
Ech.	T12	T12	T12	T3-31	T12	T12	T3-49	T3-50	T3-52	T8-87	T8-90	T14-54	T14-55	T3-30	E4e	E4e	E4e	E4e	E4e	E4e	T8e	T8e	T8e	T8e	T8e	T8e	E7e
	37	34	33		34	36						54	55	56	10	12	13	14	15	16	81	82	83	84	85	88	3
SiO_2	64.92	65.1	61.55	59.62	63.06	63.82	63.9	64.97	63.09	62.53	63.86	56.81	59.84	59.2	52.02	51.25	52.21	52.47	52.64	52.33	53.62	56.49	53.03	58.21	54.28	54.11	53.25
TiO_2	0	0.03	0	0.01	0	0	0.02	0.01	0	0.02	0.04	0.24	0.01	0.02	0.005	0.106	0.133	0.005	0.158	0.082	0.09	0.06	0.02	0.06	0.02	0.06	0
Al_2O_3	18.69	18.47	24.99	23.24	23.93	24.41	18.61	18.62	18.15	18.66	18.76	27.33	22.8	23.94	29.15	29.98	29.17	29.01	28.34	29.49	29.74	27.03	29.12	26.48	29.64	28.89	25.13
FeO	0.01	0.08	0.13	0.07	0	0.13	0.11	0.08	0	0.12	0	0.33	0	0.03	0.421	0.281	0.414	0.161	1.132	0.453	0.21	0.14	0	0.23	0.03	0.52	0.563
MnO	0.04	0.05	0	0	0.05	0.09	0	0	0.09	0.05	0.05	0.02	0	0	0	0.048	0	0.074	0.023	0.007	0.13	0	0	0	0.05	0	0
MgO	0	0	0	0.01	0.02	0	0	0	0	0	0.01	0.01	0.01	0.02	0.1	0.007	0.095	0.018	0.292	0.18	0.05	0	0.07	0	0.03	0.14	0.313
CaO	0.05	0.04	5.96	5.43	4.81	3.55	0.02	0.01	0.05	0.02	0.08	9.03	5.47	5.86	13.04	13.02	12.09	11.97	11.27	9.2	11.87	9.19	12.01	8.38	11.59	10.89	13.92
Na_2O	0.56	0.4	7.89	7.9	8.08	8.18	0.18	0.48	0.21	1.91	3.06	5.98	7.36	7.72	4.167	4.241	4.662	4.832	4.745	4.587	4.62	6.23	4.44	6.6	4.77	5.04	4.709
K_2O	16.12	16.14	0.38	0.42	0.5	0.4	16.44	16.17	16.53	13.6	12.3	0.27	0.8	0.25	0.148	0.132	0.249	0.299	0.525	2.003	0.17	0.27	0.19	0.26	0.14	0.3	0.377
Total	100.4	100.3	100.9	96.69	100.4	100.6	99.28	100.3	98.12	96.91	98.15	100	96.28	97.02	98.97	99.06	98.94	98.82	98.87	98.17	100.5	99.41	98.82	100.2	100.5	99.83	97.99
Si	6.375	6.395	5.782	5.842	5.919	5.581	6.359	6.382	6.366	6.323	6.34	5.439	5.885	5.782	5.097	5.024	5.111	5.142	5.162	5.158	5.152	5.446	5.172	5.548	5.197	5.224	5.674
Al	2.161	2.137	2.765	2.682	2.645	2.514	2.181	2.154	2.157	2.222	2.193	3.081	2.641	2.754	3.363	3.461	3.363	3.347	3.273	3.423	3.365	3.069	3.345	2.972	3.342	3.285	3.154
Ti	0	0.002	0	0.001	0	0	0.001	0.001	0	0.002	0.003	0.017	0.001	0.001	0	0.008	0.01	0	0.012	0.006	0.007	0.004	0.001	0.004	0.001	0.004	0
Fe^{2+}	0.001	0.007	0.01	0.006	0	0.01	0.009	0.007	0	0.01	0	0.026	0	0.002	0.034	0.023	0.034	0.013	0.093	0.037	0.017	0.011	0	0.018	0.002	0.042	0.05
Mn	0.003	0.004	0	0	0.004	0.007	0	0	0.008	0.004	0.004	0.002	0	0	0	0.004	0	0.006	0.002	0.001	0.011	0	0	0	0.004	0	0
Mg	0	0	0	0.001	0.003	0	0	0	0	0	0.001	0.001	0.001	0.003	0.015	0.001	0.014	0.003	0.043	0.026	0.007	0	0.01	0	0.004	0.02	0.05
Ca	0.005	0.004	0.6	0.57	0.484	0.333	0.002	0.001	0.005	0.002	0.009	0.926	0.576	0.613	1.369	1.368	1.269	1.257	1.184	0.972	1.222	0.949	1.255	0.856	1.189	1.126	1.589
Na	0.107	0.076	1.437	1.501	1.471	1.387	0.035	0.091	0.041	0.374	0.589	1.11	1.404	1.462	0.792	0.806	0.885	0.918	0.902	0.877	0.861	1.165	0.84	1.22	0.886	0.943	0.973
K	2.019	2.023	0.046	0.053	0.06	0.045	2.087	2.026	2.128	1.754	1.558	0.033	0.1	0.031	0.018	0.017	0.031	0.037	0.066	0.252	0.021	0.033	0.024	0.032	0.017	0.037	0.051
Cations	10.67	10.65	10.64	10.66	10.59	9.877	10.67	10.66	10.71	10.69	10.7	10.64	10.61	10.65	10.69	10.71	10.72	10.72	10.74	10.75	10.66	10.68	10.65	10.65	10.64	10.68	11.54
Ab	5	3.6	69	70.7	73	78.6	1.6	4.3	1.9	17.6	27.3	53.6	67.5	69.4	36.3	36.8	40.5	41.5	41.9	41.7	40.9	54.3	39.6	57.9	42.4	44.8	37.2
An	0.2	0.2	28.8	26.8	24	18.9	0.1	0	0.2	0.1	0.4	24.8	27.7	29.1	62.8	62.4	58.1	56.8	55	46.3	58.1	44.2	59.2	40.6	56.8	53.5	60.8
Or	94.7	96.2	2.2	2.5	3	2.5	98.3	95.7	97.9	82.3	72.3	2.6	4.8	1.5	0.8	0.8	1.4	1.7	3.1	12	1	1.5	1.1	1.5	0.8	1.8	2

Table 1B
Selected analyses of amphibole from the Temaguessine pluton

	Granite														Enclaves						
N° ech.	T11-16	T11-16	T11-16	T3-21	T8-25	T8-25	T8-25	T8-25	E2	E2	E2	E3	E3	E3	E7e	T8e	T8e	T8e	E4e	E4e	E4e
N° anal.	43	44	57	65	82	25	30	40	33	34	35	11	14	6	89	13	20	22	51	67	61
SiO_2	38.86	39.27	38.08	38.17	37.82	38	39.73	40.09	42.36	40.49	42.05	40.81	41.29	42.2	47.22	45.14	43.09	42.69	42.93	42.71	44.49
TiO_2	1.263	1.571	0.972	0.956	0.814	1.133	0.934	1.349	1.87	1.95	2.06	1.54	1.64	1.89	1.42	1.57	1.96	1.89	2.20	2.01	1.53
Al_2O_3	9.228	9.116	9.612	9.655	9.564	9.16	9.836	9.143	8.87	9.33	8.85	8.5	8.5	8.22	5.87	6.91	8.47	8.01	8.27	8.32	7.38
FeO	27.41	27.5	27.55	28.23	27.79	28.56	29.66	27.78	23.85	25.95	24.3	26.83	27.69	26.26	16.88	22.81	22.61	23.01	23.55	22.43	22.87
Cr_2O_3	0	0.167	0	0	0.022	0	0.012	0.041	0.06	0	0.05	0	0.08	0.02	0.00	0.03	0.00	0.14	0.05	0.00	0.06
MnO	0.465	0.48	0.589	0.5	0.739	0.567	0.684	0.051	0.59	0.55	0.62	0.62	0.4	0.52	0.29	0.37	0.38	0.51	0.44	0.45	0.32
MgO	3.402	3.644	3.23	3.154	2.91	3.092	3.235	3.164	6.49	4.72	6.13	4.69	4.5	5.32	12.37	7.60	6.67	7.01	6.65	6.78	7.82
CaO	10.2	10.23	10.46	10.32	10.47	10.54	10.96	10.7	10.68	10.77	10.66	10.91	10.67	10.59	11.43	10.86	10.84	11.47	10.77	10.87	10.97
Na_2O	1.868	1.76	1.696	1.729	1.77	1.771	1.883	1.961	1.64	1.58	1.54	1.77	1.64	1.7	1.03	1.30	1.58	1.43	1.60	1.47	1.31
K_2O	1.349	1.35	1.436	1.437	1.543	1.497	1.489	1.417	1.38	1.27	1.32	1.29	1.31	1.22	0.50	0.72	1.08	1.05	0.98	1.01	0.75
F	1.104	0.562	0.436	0.153	0.155	0.806	1.104	0.484	0.39	0.44	0.62	0.63	0.66	0.26	0.19	0.27	0.05	0.00	0.36	0.11	0.16
Cl	0.18	0.2	0.235	0.174	0.228	0.231	0.208	0.024	0.21	0.25	0.18	0.2	0.26	0.21	0.10	0.08	0.23	0.10	0.18	0.11	0.06
Total	95.32	95.69	94.29	94.48	93.8	95.36	99.73	96.15	98.33	97.3	98.33	97.79	98.56	98.39	97.28	97.62	96.96	97.17	97.93	96.28	97.66
Si	6.389	6.369	6.307	6.281	6.309	6.284	5.632	6.523	6.526	6.408	6.504	6.475	6.483	6.558	6.98	6.89	6.69	6.62	6.62	6.67	6.77
AlIV	1.611	1.631	1.693	1.719	1.691	1.716	1.642	1.477	1.474	1.592	1.496	1.525	1.517	1.442	1.02	1.11	1.31	1.38	1.38	1.33	1.23
AlVI	0.176	0.11	0.182	0.153	0.189	0.067	0	0.275	0.135	0.146	0.116	0.063	0.054	0.063	0.00	0.13	0.24	0.09	0.12	0.20	0.09
Cr	0	0.021	0	0	0.003	0	1.343	0.005	0.007	0	0.006	0	0.01	0.002	0.00	0.00	0.00	0.02	0.01	0.00	0.01
Fe_3	0.65	0.729	0.707	0.838	0.651	0.749	0.707	0.223	0.611	0.589	0.639	0.579	0.714	0.654	0.70	0.54	0.31	0.38	0.52	0.38	0.67
Ti	0.156	0.192	0.121	0.118	0.102	0.141	0.1	0.165	0.217	0.232	0.24	0.184	0.194	0.221	0.16	0.18	0.23	0.22	0.26	0.24	0.18
Mg	0.834	0.881	0.798	0.774	0.724	0.762	0.684	0.768	1.491	1.114	1.413	1.109	1.053	1.233	2.72	1.73	1.54	1.62	1.53	1.58	1.77
Fe_2	3.118	3.001	3.109	3.047	3.227	3.201	2.084	3.557	2.462	2.846	2.505	2.981	2.921	2.759	1.38	2.37	2.62	2.61	2.51	2.55	2.24
Mn	0.065	0.066	0.083	0.07	0.104	0.079	0.082	0.007	0.077	0.074	0.081	0.083	0.053	0.068	0.04	0.05	0.05	0.07	0.06	0.06	0.04
Ca	1.796	1.777	1.856	1.819	1.871	1.867	1.665	1.865	1.763	1.826	1.767	1.855	1.795	1.763	1.81	1.78	1.80	1.91	1.78	1.82	1.79
NaB	0.204	0.223	0.144	0.181	0.129	0.133	0.335	0.135	0.237	0.174	0.233	0.145	0.205	0.237	0.19	0.22	0.20	0.09	0.22	0.18	0.21
Na	0.392	0.331	0.401	0.37	0.444	0.435	0.183	0.484	0.253	0.311	0.228	0.399	0.294	0.276	0.11	0.16	0.28	0.34	0.26	0.26	0.18
K	0.283	0.279	0.303	0.302	0.328	0.316	0.269	0.294	0.271	0.256	0.26	0.261	0.262	0.242	0.09	0.14	0.21	0.21	0.19	0.20	0.15
Cations	15.68	15.61	15.71	15.67	15.77	15.75	15.45	15.78	15.52	15.57	15.49	15.66	15.56	15.52	15.20	15.30	15.49	15.55	15.45	15.47	15.32
XMg	0.21	0.23	0.2	0.2	0.18	0.19	0.25	0.18	0.38	0.28	0.36	0.27	0.26	0.31	0.66	0.42	0.37	0.38	0.38	0.38	0.44
XFe	0.79	0.77	0.8	0.8	0.82	0.81	0.75	0.82	0.62	0.72	0.64	0.73	0.74	0.69	0.34	0.58	0.63	0.62	0.62	0.62	0.56
Ti temp.	732	777	683	678	654	711	650	743	806	823	832	767	779	811	733	762	820	810	849	828	756

Table 1C
Selected analyses of biotite from the Temaguessine pluton

Faciès	Biotite granite								Orbicule	Amphibole–biotite granite							Xenolith		Enclaves								
N°samp	E1a	T12	T12	T12	T12	T12	T12	T12	T12e	E7	E7	E7	T8	T8	T8	T8	T14	T14	T10e	T10e	T10e	E4e	E4e	E4e	E4e	T8e	T8e	T8e
N°anal.	28	1	15	17	22	25	28	30	12	3	7	8	31	39	26	27	40	43	14	15	23	49	50	83	85	7	23	56
SiO_2	34.93	35.23	34.68	36.52	34.18	34.98	33.72	34.7	34.73	34.64	35.17	35.53	35.31	34.59	34.46	33.12	35.9	35.74	34.46	34.72	34.3	35.41	35.2	34.89	35.24	35.84	35.43	34.83
Al_2O_3	17.24	18.77	19.06	19.78	19.57	19.4	19.28	19.49	18.59	13.47	13.46	13.33	12.76	12.68	12.7	13.19	13.43	13.09	12.93	13.26	13.14	12.89	12.95	13.12	12.86	12.94	13.11	13.05
TiO_2	2.65	3.37	3.85	3.52	3.1	3.17	2.64	3.2	3.69	4.02	4.77	4.87	4.14	3.63	3.7	3.23	4.1	4.26	3.63	3.78	3.5	5.189	5.504	5.062	4.896	4.88	5.09	5.11
FeO	24.72	23.44	24.41	23.77	26.14	25.59	27.72	27.19	23.97	24.45	24.25	23.24	30.77	28.43	29.44	31.94	20.36	20.98	27.27	27.59	27.23	26.17	26.28	26.51	25.59	25.24	25.24	23.68
MnO	0.43	0.58	0.29	0.36	0.54	0.47	0.26	0.27	0.32	0.24	0.34	0.22	0.34	0.26	0.21	0.42	0.22	0.24	0.44	0.52	0.42	0.227	0.13	0.076	0.178	0.08	0.27	0.22
MgO	5.68	3.17	3.1	3.59	3.37	3.25	3.32	3.16	3.27	9.3	8.5	8.82	4.58	4.42	4.55	4.64	9.61	9.43	4.71	4.74	4.42	7.103	6.974	6.854	7.294	7.67	7.4	7.39
CaO	0	0.03	0.07	0.06	0	0.03	0.06	0	0.08	0	0.06	0.01	0.06	0.03	0.01	0.06	0.03	0.19	0.04	0.07	0.03	0	0.07	0.077	0.109	0	0.06	0.05
Cr_2O_3	0	0	0.11	0	0	0.21	0.05	0	0.08	0	0.04	0	0	0.04	0.07	0.05	0.02	0.09	0.04	0.13	0.04	0	0.124	0.061	0.035	0	0.04	0
Na_2O	0.16	0.16	0.16	0.23	0.16	0.15	0.07	0.08	0.17	0.1	0.12	0.18	0.09	0.11	0.06	0.11	0.15	0.11	0.07	0.08	0.06	0.1	0.086	0.053	0.071	0.11	0.17	0.11
K_2O	9.08	9.44	9.25	9.46	9.23	9.22	9.18	9.29	9.14	8.73	9.66	9.12	8.92	9.04	8.21	6.68	9.09	9.05	8.72	8.83	9.38	8.826	9.29	9.11	8.562	9.06	8.9	9.17
F	0.93	1.11	0.82	0.87	0.4	0.28	0.32	0.27	0.31	0.49	0.85	0.4	0.54	0.67	0.3	0.44	0.51	0.45	0.51	0.61	0.31	0.237	0.368	0.086	0.322	0	0.51	0
Cl	0.15	0.13	0.21	0.17	0.12	0.15	0.12	0.15	0.13	0.12	0.13	0.14	0.14	0.21	0.1	0.21	0.02	0.07	0.28	0.23	0.2	0.199	0.087	0.136	0.16	0.14	0.17	0.11
Total	95.97	95.43	96.01	98.33	96.81	96.9	96.74	97.8	94.48	95.56	97.35	95.86	97.65	94.11	93.81	94.09	93.44	93.7	93.1	94.56	93.03	96.35	97.06	96.02	95.31	95.96	96.39	93.72
Si	5.498	5.546	5.435	5.535	5.333	5.420	5.303	5.363	5.49	5.470	5.490	5.555	5.625	5.696	5.662	5.483	5.672	5.656	5.69	5.65	5.68	5.57	5.52	5.52	5.59	5.62	5.57	5.58
AlIV	2.502	2.454	2.565	2.465	2.667	2.580	2.697	2.637	2.51	2.507	2.476	2.445	2.375	2.304	2.338	2.517	2.328	2.344	2.31	2.35	2.32	2.39	2.39	2.45	2.40	2.38	2.43	2.42
AlVI	0.696	1.029	0.955	1.068	0.932	0.963	0.876	0.913	0.95	0.000	0.000	0.011	0.021	0.157	0.121	0.057	0.173	0.097	0.21	0.20	0.24	0.00	0.00	0.00	0.00	0.01	0.00	0.04
Cr	0.000	0.000	0.014	0.000	0.000	0.026	0.006	0.000	0.01	0.000	0.005	0.000	0.000	0.005	0.009	0.007	0.002	0.011	0.01	0.02	0.01	0.00	0.02	0.01	0.00	0.00	0.00	0.00
Fe	3.254	3.086	3.199	3.013	3.411	3.316	3.646	3.514	3.17	3.229	3.166	3.039	4.100	3.915	4.045	4.422	2.690	2.777	3.77	3.76	3.77	3.44	3.45	3.51	3.39	3.31	3.32	3.17
Mg	1.333	0.744	0.724	0.811	0.784	0.751	0.778	0.728	0.77	2.189	1.978	2.055	1.088	1.085	1.114	1.145	2.263	2.224	1.16	1.15	1.09	1.67	1.63	1.62	1.72	1.79	1.73	1.76
Mn	0.057	0.077	0.038	0.046	0.071	0.062	0.035	0.035	0.04	0.032	0.045	0.029	0.046	0.036	0.029	0.059	0.029	0.032	0.06	0.07	0.06	0.03	0.02	0.01	0.02	0.01	0.04	0.03
Ti	0.314	0.399	0.454	0.401	0.364	0.369	0.312	0.372	0.44	0.477	0.560	0.573	0.496	0.450	0.457	0.402	0.487	0.507	0.45	0.46	0.44	0.61	0.65	0.60	0.58	0.58	0.60	0.62
Y	5.653	5.336	5.384	5.339	5.561	5.487	5.653	5.562	5.38	5.927	5.753	5.706	5.750	5.649	5.775	6.091	5.645	5.648	5.66	5.66	5.60	5.75	5.76	5.74	5.73	5.69	5.69	5.62
Ca	0.000	0.005	0.012	0.010	0.000	0.005	0.010	0.000	0.01	0.000	0.010	0.002	0.010	0.005	0.002	0.011	0.005	0.032	0.01	0.01	0.01	0.00	0.01	0.01	0.02	0.00	0.01	0.01
Na	0.049	0.049	0.049	0.068	0.048	0.045	0.021	0.024	0.05	0.031	0.036	0.055	0.028	0.035	0.019	0.035	0.046	0.034	0.02	0.03	0.02	0.03	0.03	0.02	0.02	0.03	0.05	0.03
K	1.823	1.896	1.849	1.829	1.837	1.823	1.842	1.832	1.84	1.759	1.924	1.819	1.813	1.899	1.721	1.411	1.832	1.827	1.84	1.83	1.98	1.77	1.86	1.84	1.73	1.81	1.78	1.87
F	0.463	0.553	0.406	0.417	0.197	0.137	0.159	0.132	0.15	0.245	0.420	0.198	0.272	0.349	0.156	0.230	0.255	0.225	0.27	0.31	0.16	0.12	0.18	0.04	0.16	0.00	0.25	0.00
Cl	0.040	0.035	0.056	0.044	0.032	0.039	0.032	0.039	0.03	0.032	0.034	0.037	0.038	0.059	0.028	0.059	0.005	0.019	0.08	0.06	0.06	0.05	0.02	0.04	0.04	0.04	0.05	0.03
X	1.872	1.950	1.909	1.906	1.885	1.873	1.873	1.855	1.91	1.789	1.970	1.875	1.851	1.939	1.742	1.457	1.883	1.893	1.87	1.87	2.00	1.80	1.90	1.87	1.77	1.84	1.85	1.92
Cations	15.525	15.285	15.293	15.246	15.447	15.360	15.526	15.418	15.29	15.694	15.689	15.581	15.601	15.588	15.517	15.548	15.528	15.541	15.52	15.53	15.60	15.52	15.57	15.58	15.50	15.54	15.53	15.53
X Mg	0.291	0.194	0.185	0.212	0.187	0.185	0.176	0.172	0.20	0.404	0.385	0.403	0.210	0.217	0.216	0.206	0.457	0.445	0.24	0.23	0.22	0.33	0.32	0.32	0.34	0.35	0.34	0.36
XFe	0.709	0.806	0.815	0.788	0.813	0.815	0.824	0.828	0.80	0.596	0.615	0.597	0.790	0.783	0.784	0.794	0.543	0.555	0.76	0.77	0.78	0.67	0.68	0.68	0.66	0.65	0.66	0.64

Table 1D
Selected analyses of orthopyroxene from the Temaguessine pluton

Sample	E4-e1-1	E4-e1-2	E4-e1-5	E4-e1-6	E4-e1-7	E4-e1-8	E4-e1-9	T8E-1	T8E-3	T8E-4
SiO_2	52.941	52.558	52.62	51.841	51.499	51.766	51.118	52.69	52.22	52.63
TiO_2	0.567	0.504	0.394	0.554	0.454	0.605	0.617	0.49	0.43	0.5
Al_2O_3	1.523	1.493	1.393	2.105	1.717	1.466	1.466	1.7	1.83	1.73
FeO	20.827	21.945	19.822	19.43	20.554	22.422	22.323	20.02	20.79	20.34
Cr_2O_3	0.197	0.304	0.225	0.324	0.243	0.196	0.232	0	0.13	0.22
MnO	0.318	0.363	0.433	0.293	0.382	0.484	0.44	0.12	0.41	0.26
MgO	22.24	21.324	22.667	22.924	22.48	21.097	21.736	22.95	22.31	22.38
CaO	1.773	1.602	1.867	1.678	1.679	1.766	1.811	1.79	1.53	1.69
Na_2O	0	0	0	0.036	0.039	0	0.028	0.04	0.03	0.02
K_2O	0	0.023	0	0	0	0	0.023	0	0	0.01
Total	100.39	100.12	99.42	99.19	99.05	99.8	99.79	99.8	99.68	99.78
Si	1.96	1.962	1.958	1.928	1.926	1.942	1.912	1.949	1.943	1.955
AlIV	0.04	0.038	0.042	0.072	0.074	0.058	0.065	0.051	0.057	0.045
AlVI	0.026	0.028	0.02	0.021	0.002	0.007	0	0.024	0.023	0.031
Ti	0.016	0.014	0.011	0.016	0.013	0.017	0.017	0.014	0.012	0.014
Cr	0.006	0.009	0.007	0.010	0.007	0.006	0.007	0.000	0.004	0.006
Mg	1.227	1.187	1.258	1.271	1.253	1.180	1.212	1.266	1.238	1.240
Fe_2	0.645	0.685	0.617	0.604	0.643	0.704	0.698	0.619	0.647	0.632
Mn	0.010	0.011	0.014	0.009	0.012	0.015	0.014	0.004	0.013	0.008
Ca	0.070	0.064	0.074	0.067	0.067	0.071	0.073	0.071	0.061	0.067
Na	0.000	0.000	0.000	0.003	0.003	0.000	0.002	0.003	0.002	0.001
K	0.000	0.001	0.000	0.000	0.000	0.000	0.001	0.000	0.000	0.000
Ca	3.602	3.290	3.793	3.426	3.405	3.604	3.635	3.620	3.115	3.455
Mg	62.863	60.939	64.077	65.132	63.442	59.901	60.697	64.583	63.191	63.665
Fe_2_Mn	33.535	35.771	32.130	31.442	33.153	36.495	35.668	31.797	33.694	32.880
WO	3.602	3.290	3.793	3.426	3.405	3.604	3.635	3.620	3.115	3.455
EN	62.863	60.939	64.077	65.132	63.442	59.901	60.697	64.583	63.191	63.665
FS	33.535	35.771	32.130	31.442	33.153	36.495	35.668	31.797	33.694	32.880

Table 1E
Analyses of cordierite from the orbicules in the Temaguessine pluton

Sample	Te12-1	Te12-2	Te12-3	Te12-4	E1e-5	E1e-6	E1e-7	E1e-8	E1e-9	E1e-10	E1e-11	E1e-12	E1e-13	E1e-14	E1e-15
SiO_2	45.94	44.76	46.11	45.6	45.3	45	44.94	42.14	44.42	45.16	44.76	44.66	44.65	43.02	45.87
TiO_2	0.00	0.00	0.08	0.01	0.04	0.01	0.00	0.00	0.00	0.00	0.00	0.05	0.00	0.00	0.01
Al_2O_3	30.79	28.56	30.26	30.52	28.23	28.15	28.33	26.73	28.64	27.72	28.56	28.69	28.14	28.49	29.14
Cr_2O_3	0.00	0.00	0.00	0.00	0.00	0.00	0.00	0.00	0.00	0.00	0.00	0.00	0.00	0.00	0.00
FeO	14.70	16.92	14.94	14.39	17.59	17.53	16.14	14.86	17.50	16.53	16.92	17.79	16.48	17.34	16.13
MnO	0.99	0.96	1.32	0.85	1.143	0.94	1.12	0.69	0.96	1.61	0.96	0.91	1.08	1.02	0.94
MgO	2.36	1.78	2.4	2.31	1.538	1.53	2.2	1.66	1.78	1.89	1.78	1.54	2.04	1.86	2.33
CaO	0.07	0.09	0.12	0.07	0.106	0.12	0.06	0.39	0.16	0.1	0.09	0.23	0.11	0.19	0.06
Na_2O	1.15	1.37	1.24	0.98	1.405	1.38	1.22	0.57	1.37	1.32	1.37	1.37	1.33	0.87	1.38
K_2O	0.03	0.01	0.03	0.57	0.076	0.02	0.63	4.24	0.04	0.04	0.01	0.07	0	1.77	0.04
Total	96.03	94.45	96.5	95.3	95.43	94.68	94.64	91.28	94.87	94.37	94.45	95.31	93.83	94.56	95.90
Si	5.03	5.06	5.04	5.04	5.09	5.09	5.07	5.03	5.02	5.12	5.06	5.03	5.08	4.94	5.08
Al	3.79	3.80	3.90	3.97	3.73	3.75	3.76	3.76	3.81	3.70	3.80	3.80	3.77	3.85	3.80
Ti	0.00	0.00	0.01	0.00	0.00	0.00	0.00	0.00	0.00	0.00	0.00	0.00	0.00	0.00	0.00
Fe_2	1.34	1.6	1.36	1.33	1.65	1.66	1.52	1.48	1.65	1.56	1.6	1.67	1.56	1.66	1.49
Fe_3	0.00	0.00	0.00	0.00	0.00	0.00	0.00	0.00	0.00	0.00	0.00	0.00	0.00	0.00	0.00
Mn	0.09	0.09	0.12	0.08	0.1	0.09	0.1	0.07	0.09	0.15	0.09	0.08	0.1	0.09	0.08
Mg	0.38	0.3	0.39	0.38	0.25	0.25	0.37	0.29	0.3	0.31	0.3	0.25	0.34	0.31	0.38
Ca	0.00	0.01	0.01	0.00	0.01	0.01	0.00	0.05	0.01	0.01	0.01	0.02	0.01	0.02	0.00
Na	0.24	0.3	0.26	0.21	0.3	0.3	0.26	0.13	0.3	0.29	0.3	0.29	0.29	0.19	0.29
K	0.00	0.00	0.00	0.08	0.01	0.00	0.09	0.64	0.00	0.00	0.00	0.01	0.00	0.25	0.00
Total	11.09	11.17	11.12	10.77	11.18	11.17	11.21	11.47	11.21	11.17	11.17	11.2	11.17	11.35	11.16
XFe	0.8	0.8	0.8	0.7	0.9	0.9	0.8	0.8	0.9	0.8	0.8	0.9	0.8	0.8	0.8
$100 * X_{Mg}$	21	15	21	21	13	13	19	16	15	15	15	13	17	15	19

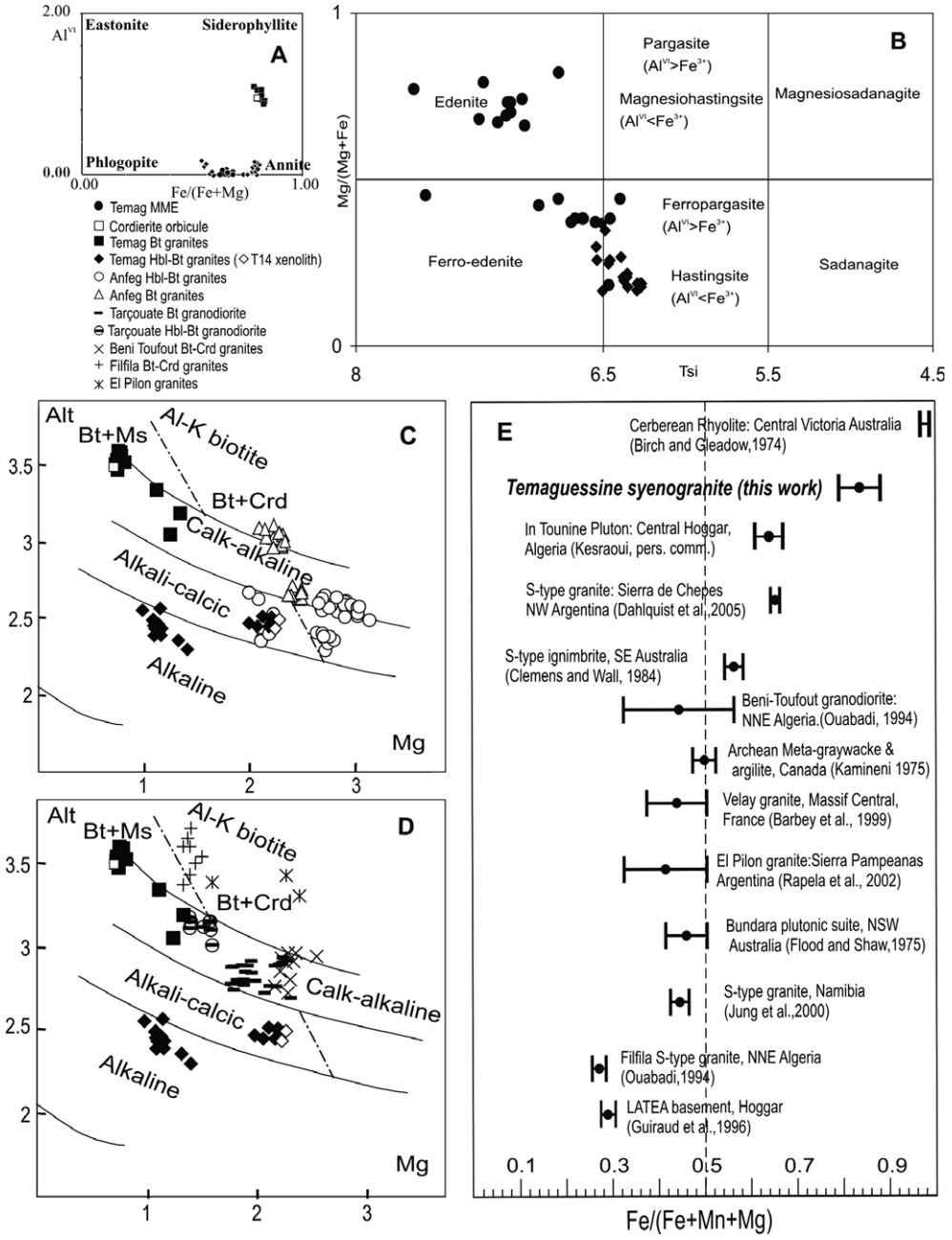

Fig. 4. Selected mineralogical characteristics from the Temaguessine rocks: (A) Composition of the Temaguessine biotite after Guidotti, 1984. (B) compositions of the Temaguessine amphiboles after Leake et al. (1997); (C) Mg–Al_t diagram (Nachit et al., 1985) of the biotites from the different Temaguessine facies compared with those of the Anfeg batholith (Hoggar, Acef et al., 2003); (D) Mg–Al_t diagram (Nachit et al., 1985) of the biotites from the Temaguessine biotite syenogranite compared with those of the Tarçouate pluton (Morocco, Barbey et al., 2001), the Beni-Toufout and Filfila plutons (Northern Algeria, Ouabadi, 1994) and the El-Pilon pluton (Argentina, Rapela et al., 2002); and (E) Comparison of the X_{Fe} values of the Temaguessine cordierite with other cordierite-bearing lithologies in Hoggar and other rocks in the world having Fe-rich cordierite (See above mentioned references for further information).

syenogranite and from the cordierite orbicule is highly aluminous (Al_{tot} between 2.3 and 3.5), plotting at the boundary between the peraluminous and the calc-alkaline granite fields; (2) the biotite from the biotite–amphibole granite is much less aluminous and plot in the alkali-calcic field or even in the alkaline field for the less magnesian group. The latter have an Al_{tot} content similar to the biotite of the Anfeg batholith (Acef et al., 2003), but lower Mg content (MgO < 1.5), indicating an alkaline affinity, in agreement with the general characteristics of the Hoggar late circular plutons (Azzouni-Sekkal et al., 2003; Bonin et al., 1998; Liégeois and Black, 1987). The T14 xenolith whose REE indicate that it came from the enclosing Anfeg-type batholith (see below), has the biotite with the highest Mg content, i.e. the closest to the Anfeg biotite compositions.

Table 2
U–Pb SHRIMP data for the Temaguessine pluton (sample F13)

Spot name	% comm ^{206}Pb	ppm U	ppm Th	^{232}Th/^{238}U	ppm Rad ^{206}Pb	^{238}U/^{206}Pbr	1σ% err	^{207}Pbr/^{206}Pbr	1σ% err	^{207}Pbr/^{235}U	1σ% err	^{206}Pbr/^{238}U	1σ% err	Err corr	^{206}Pbr/^{238}U age	1σ% err
f13-01	0.74	637	362	0.59	51.7	10.673	1.14	0.0637	2.12	0.823	2.40	0.0937	1.14	0.473	574	6
f13-02	0.18	411	275	0.69	33.0	10.721	1.19	0.0621	1.42	0.798	1.86	0.0933	1.19	0.643	573	7
f13-03	0.02	630	466	0.76	50.4	10.740	1.13	0.0604	0.90	0.776	1.44	0.0931	1.13	0.782	573	6
f13-04	0.45	872	376	0.45	74.5	10.095	1.10	0.0871	1.80	1.190	2.11	0.0991	1.10	0.522	591	6
f13-05	0.05	652	348	0.55	53.1	10.560	1.13	0.0603	1.50	0.787	1.88	0.0947	1.13	0.602	583	6
f13-06	0.04	673	583	0.90	54.9	10.536	1.13	0.0632	0.99	0.827	1.50	0.0949	1.13	0.753	582	6
f13-07	0.02	345	206	0.62	27.9	10.628	1.23	0.0650	1.43	0.844	1.89	0.0941	1.23	0.653	576	7
f13-08	0.23	1155	468	0.42	95.7	10.400	1.12	0.0748	1.50	0.992	1.88	0.0962	1.12	0.600	582	6
f13-09	0.13	395	207	0.54	31.9	10.643	1.20	0.0595	1.33	0.771	1.80	0.0940	1.20	0.671	579	7
f13-10	0.00	3422	3672	1.11	293.3	10.022	1.02	0.0599	0.35	0.824	1.08	0.0998	1.02	0.945	613	6
f13-11c	0.11	865	380	0.45	70.8	10.517	1.09	0.0604	1.16	0.791	1.59	0.0951	1.09	0.687	585	6
f13-11r	0.85	720	338	0.48	60.3	10.333	1.11	0.0857	4.69	1.144	4.82	0.0968	1.11	0.231	578	7
f13-12	0.28	643	241	0.39	55.7	9.946	1.96	0.0846	5.66	1.173	5.99	0.1005	1.96	0.327	601	12
f13-13	1.37	314	171	0.56	26.5	10.333	1.25	0.0676	3.45	0.902	3.67	0.0968	1.25	0.341	590	7
f13-14c	0.08	2669	1291	0.50	223.6	10.262	1.04	0.0628	1.15	0.844	1.55	0.0975	1.04	0.673	597	6
f13-14r	0.58	966	385	0.41	64.9	12.859	1.09	0.0820	1.33	0.880	1.72	0.0778	1.09	0.633	469	5
f13-15c	0.80	209	124	0.61	55.2	3.276	0.60	0.1076	1.55	4.531	1.66	0.3053	0.60	0.360	1713	10
f13-16c	0.28	95	53	0.57	27.4	2.991	0.81	0.1258	1.15	5.797	1.41	0.3343	0.81	0.575	1834	15
f13-17c	0.06	378	269	0.73	101.6	3.198	0.45	0.1145	0.45	4.935	0.63	0.3127	0.45	0.708	1740	8
f13-18c	0.13	201	131	0.67	53.9	3.208	3.29	0.1148	0.54	4.935	3.33	0.3117	3.29	0.987	1734	56

The Temaguessine biotites have been compared with three other comparable granites, either because they comprise cordierite (Northern Algeria; Argentina) or because of a similar geotectonic setting (Morocco).

In northern Algeria, the Cenozoic magmatism comprises some cordierite-bearing granitoids (Ouabadi, 1994; Fourcade et al., 2001). The main metaluminous high-K calc-alkaline magmatism is coeval with strongly peraluminous granitoids. Among the latter, two plutons contain cordierite but their origins are dissimilar: the Filfila pluton was derived directly from the partial melting of metasediments leading to peraluminous magma while the Béni-Toufout pluton was initially metaluminous and acquired its peraluminous character by assimilating pelitic country-rocks, still present as xenoliths (Fourcade et al., 2001). Biotites in these plutons also have a contrasted geochemistry (Fig. 4D): the Filfilla biotite belongs to the peraluminous field of Nachit et al. (1985) and the Béni-Toufout biotite to the calc-alkaline field.

In Argentina, orbicular and massive cordieritite bodies are genetically associated with highly peraluminous cordierite granitoids (El Pilon granite complex; Rapela et al., 2002). The El Pilon granitic magma was formed by anatexis of mid-crustal metamorphic rocks; a fall of the liquidus temperature of the melt during emplacement was triggered by the assimilation of surrounding hydrous metapelitic schists, followed by isobaric crystallization. The El Pilon cordierite orbicules are considered to be mafic cumulative rocks that crystallized from an isotopically homogeneous strongly peraluminous magma (Rapela et al., 2002). The El Pilon biotite is aluminous and falls within the peraluminous field (Fig. 4D).

The Tarçouate pluton (Anti-Atlas, Morocco; Barbey et al., 2001), is an inversely zoned laccolith emplaced 583 Ma ago into low-grade Eburnian (c. 2 Ga) metasediments with the following succession: leucocratic granite, biotite granodiorite/monzogranite, biotite–hornblende granodiorite/monzogranite. The Tarçouate pluton does not bear cordierite but shows the same shift in Al content between the Hb–Bi and Bi granites, the biotite from the biotite syenogranite being more enriched in Al (Fig. 4D). Chemical and isotopic compositions show that these two granitoids are likely to have been generated from the differentiation of a common parental magma by fractional crystallization, combined with a greater assimilation of pelitic schist for the biotite syenogranite, explaining the higher alumina content of its biotite (Barbey et al., 2001).

5. Condition of crystallization

Using Al-in amphibole geobarometers (Hollister et al., 1987; Schmidt, 1992), the Temaguessine amphibole would have crystallized at a pressure of 0.3–0.4 GPa, giving a maximum pressure of emplacement. Phase relationships (Clemens and Wall, 1981; Grant, 1985; Vielzeuf and Holloway, 1988; Vielzeuf and Montel, 1994) show that cordierite can be formed by melting–dehydration of biotite

at pressures ⩽0.4 GPa or can crystallize from peraluminous granitic melts in a pressure range of 0.1–0.2 GPa. In their study of the contact metamorphism of the Manaslu granite (Central Nepal), Guillot et al. (1995) used the absence of Fe-cordierite in the staurolite-bearing gneisses to deduce that the pressure remained above 0.32 GPa during granite emplacement based on the reaction Grt + Crd ⇒ St + Bi, occurring at this pressure (Thompson, 1976).

The Ti in amphibole thermometer for calcic amphiboles (Féménias et al., 2006) gives a large temperature range between 650 and 830 °C (Table 1C). Considering the titanite often associated with the amphibole, the lower calculated temperatures reflect most probably a late magmatic reequilibration. The initial magmatic temperature can thus be considered to have been at 800–830 °C. This is confirmed by the zircon saturation thermometer in whole rock (Watson and Harrison, 1983) that gives temperatures between 780 and 850 °C.

The richness in iron of the cordierite is attributed to a relatively low pressure and high water content (Birch and Gleadow, 1974; Harley et al., 2002). The absence of almandine and sillimanite within the Temaguessine Fe-cordierite orbicules indicates a pressure <0.3–0.4 GPa (Skippen and Gunter, 1996) or most probably <0.25 GPa at 800 °C and <0.2 GPa at 700 °C (Pattison et al., 1996). On the other hand, the Fe–biotite can generate Fe-cordierite at 0.3 GPa/750 °C and at 0.4 GPa/800 °C (Pattison et al., 1996). The composition and the environment of the Temaguessine cordierite strongly suggest that they are rich in H_2O (probably 1.6–1.8% H_2O; Harley et al., 2002), which would explain in part the fact that the sums of the Temaguessine cordierite analyses are around 96% (Table 1). These P–T conditions are close to the 650–700 °C and 0.3 GPa estimation for the retrogression/hydration observed in the LATEA basement in response to the emplacement of the Anfeg-type granitic batholiths (Guiraud et al., 1996).

We can then consider that the Temaguessine pluton emplacement and the generation of the cordierite orbicules occurred at about 800 °C and 0.2–0.3 GPa.

6. U–Pb zircon geochronology of the Temaguessine pluton

6.1. Analytical techniques

The U–Pb dates have been obtained on the ion microprobe (Perth Consortium SHRIMP-II) from the Geochronological laboratory of the Curtin University of Technology in Perth, Western Australia. The zircons have been polished together with the zircon standards CZ3 and TEMORA-2 ($U = 551$ ppm, ca. 120 ppm, ages = 564, 418 Ma, respectively; Black et al., 2004; Pidgeon et al., 1994). The mounted zircons were analyzed under the following conditions: cycles of 7 scans, primary O^{2-} beam of ~2 nA, spot size of ~25 μm with a mass resolution of about 5000. The data have been reduced following the procedure described by Nelson (1997) using the software SQUID (Ludwig, 2001). U/Pb ratios and U concentrations of the samples have been normalised to the TEMORA-2

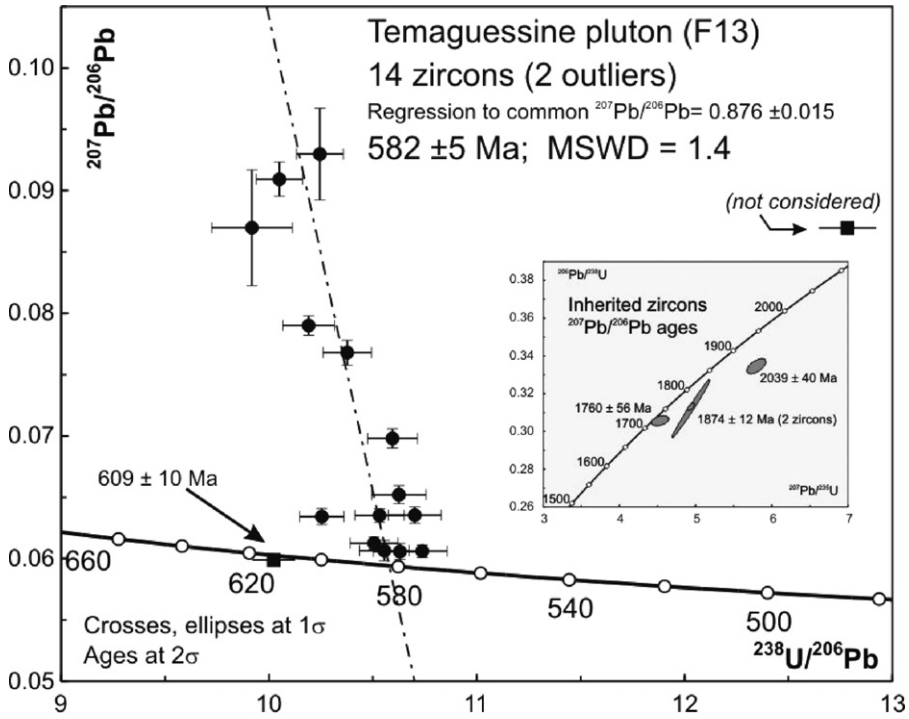

Fig. 5. U–Pb zircon SHRIMP Concordia diagram for the Temaguessine granite (Terra-Wasserburg diagram for the Pan-African zircons, normal Concordia diagram for the Palaeoproterozoic zircons).

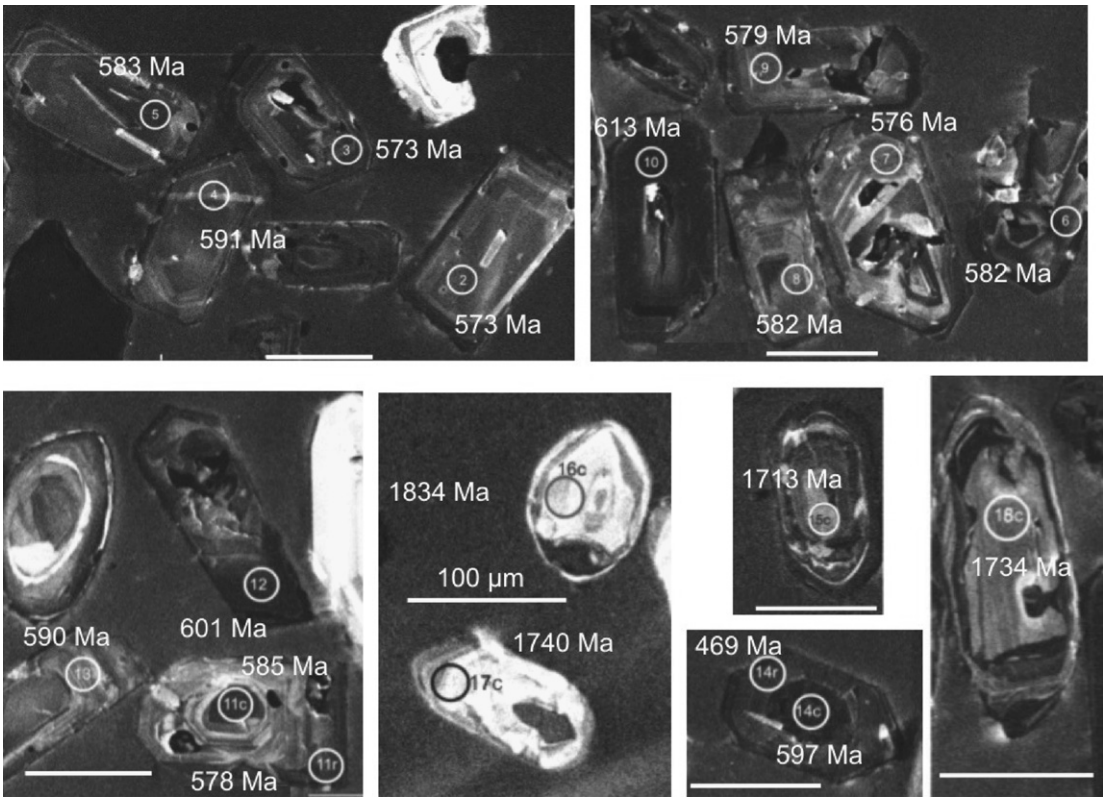

Fig. 6. Internal structures of the studied zircons with the SHRIMP spots. The white bar represents 100 µm in all pictures. The indicated ages are $^{206}Pbr/^{238}U$ ages.

and CZ3 standards, respectively. The ages have been calculated using the Isoplot/Ex, version 3.31 software (Ludwig, 2003). The results are given in Table 2. Considering the low ^{204}Pb amount and consequent larger errors on this isotope, we prefer to use for these relatively young samples uncorrected $^{207}Pb/^{206}Pb$ and $^{206}Pb/^{238}U$ ratios for display in a Tera-Wasserburg diagram and regressed the points towards calculated common Pb (Stacey and Kramers, 1975) for the age of the sample. The uncorrected data do show a small and expected drift to ancient common Pb, indicating that the regressions are valid, even when most data plot close to Concordia.

6.2. U–Pb zircon age results

Twenty spots have been measured in the zircons of the Temaguessine pluton, both in the cores and rims of the zircon crystals. Fourteen rims and cores define an age of 582 ± 5 Ma (MSWD = 1.4; Fig. 5), eight of which are nearly concordant and have a very low common lead content (<0.02% ^{206}Pb; Table 2); the other spots have a common ^{206}Pb proportion between 0.023% and 1.370%. This age is considered as the age of emplacement of the Temaguessine pluton. A large dark crystal (spot 10) gives an older age of 609 ± 10 Ma. This age corresponds to that of the Anfeg batholith (608 ± 7 Ma; Bertrand et al., 1986; recalculated by Acef et al., 2003; Fig. 1), similar to the nearby Azrou n'Fad batholith and could then represent a zircon xenocryst from an equivalent at depth of this batholith. The high content in U (3422 ppm) and in Th (3672 ppm) of this zircon (in the absence of bright U–Th inclusions in the cathodoluminescence picture; Fig. 6) could shed some doubts on the meaning of this age; however, the fact that this spot is concordant and recorded no common Pb within error limits suggests this age can be considered as meaningful. A single rim (spot 14r) gave a young age (468 ± 10 Ma) but is relatively discordant (0.58% common ^{206}Pb). This age corresponds to the beginning of the deposition of the Tassilis Ordovician sandstone. A similar young age has already been evidenced by a good 11 WR Rb–Sr isochron (482 ± 11 Ma, MSWD = 0.72; Azzouni-Sekkal et al., 2003) for the Teg'Orak Taourirt pluton. This was interpreted as a result of the fluid circulation that occurred during the reactivation of the shear zones and the initiation of the Tassilis deposition (Beuf et al., 1971). Finally, four spots are yielding older ages: $^{207}Pb/^{206}Pb$ ages are 1760 ± 56 Ma (spot 15 c), 1874 ± 12 Ma (spots 17c and 18c) and 2039 ± 40 Ma (spot 16c). Ages in the range 1.85–1.90 Ga (Peucat et al., 2003) and around 2 Ga (Bertrand et al., 1986) are known in the LATEA basement. No ages of c. 1.76 Ga are known but one must note that the ages on the LATEA basement are very scarce and that an age of 1755 ± 10 Ma is known in the basement of western Hoggar (Caby and Andreopoulos-Renaud, 1983). These different old ages can then be ascribed to the source of the Temaguessine granite.

Table 3
Whole-rock geochemistry (major and trace elements) for the Temaguessine pluton

	Amphibole–biotite granite						MME				Dykes			Biotite syenogranite Orbicule				
	T3	T6	T11	T14	E4	E9	T8E	E4e1	E3-e1	E7e	S	T9	T13	T5	T4	T12	E1a	E1e
SiO_2	73.15	71.05	69.07	68.8	73.39	74.29	58.25	57.6	53.98	49.62	58.67	60.88	54.71	71.19	79.28	74.01	73.33	67.95
TiO_2	0.28	0.52	0.78	0.63	0.2	0.7	1.7	1.74	1.65	1.22	0.84	1.01	0.76	0.35	0.28	0.18	0.16	0.14
Al_2O_3	13.37	13.17	12.8	15.1	13.06	15.8	14.85	15	15.29	15.99	15.5	14.86	15.19	14.23	9.87	13.97	13.61	15.81
Fe_2O_3t	2.56	3.78	6.45	3.45	2.43	5.42	9.7	10.82	11.22	10.53	8.06	7.78	8.22	2.79	2.43	1.78	1.84	9.76
MnO	0.02	0.03	0.06	0.04	0	0.05	0.12	0.15	0.18	0.15	0.13	0.1	0.14	0.02	0.02	0.03	0	0.45
MgO	0.25	0.54	0.85	1.13	0.2	0.74	2.78	2.8	3.45	6.5	3.63	2.85	5.92	0.37	0.27	0.21	0.22	0.94
CaO	1.34	1.49	2.04	2.49	1	2.74	5.15	5.58	6.61	8.84	6.24	4.66	8.17	1.49	1.12	0.9	0.99	0.74
Na_2O	2.57	2.3	2.72	3.39	2.56	2.84	2.91	2.9	3.06	2.55	2.73	2.64	2.85	2.65	2.03	2.82	2.81	1.38
K_2O	5.81	6.06	3.96	4.11	6.2	5.93	3.09	2.8	3.17	2.32	3.14	3.53	2.11	5.87	3.85	5.77	5.44	1.02
P_2O_5	0.01	0.12	0.19	0.16	0	0.17	0.56	0.42	0.34	0.24	0.14	0.22	0.09	0.14	0.08	0.06	0.06	0.1
Loss	0.48	0.83	0.97	0.69	0.77	0.74	0.88	0.53	0.94	2.14	1.42	1.36	1.72	0.81	0.59	0.7	1.33	1.45
Total	99.84	99.89	99.89	99.99	99.81	99.42	99.99	100.3	99.89	100.1	100.5	99.89	99.88	99.91	99.82	100.4	99.79	99.74
As	1.07	0.81	0.73		0.76	1.12	1.44	1.26	1.07	0.65	0.84	0.77	0.66	0.82	1.31	1.29	0.83	1.71
Ba	538	687	297	1570	456	1863	1026	1224	575	696	333	530	174	874	330	399	363	110
Be	2.88	1.85	4.64	3.24	3.14	2.09	2.53	2.06	2.54	1.42	1.72	2.36	3.54	3.46	2.41	7.55	2.7	1431
Bi	0.15	0.43	0.08	0.08	0.65		0.14			0.09	0.13	0.33	0.32		0.1	0.08		
Co	3.1	6.06	8.31	8.59	2.67	8.66	25.6	27.6	33.5	43.6	25.1	24	34.3	3.73	2.9	1.61	2.25	5.13
Cr	14.8	21.4	13.6	47.9	349	385	68	324	159	159	268	34.7	347	9.6	20.2	17	158	1066
Cs	6.57	3.57	6.69	1.77	3.64	2.79	3.31	1.68	2.19	1.03	5.87	4.44	4.35	4.74	5.35	10.6	10.2	93
Cu		21.9		10.5		7.3	38.2	41.6	52.1	12.5	16.3	23.7	7.3					11.1
Ga	22.4	21	28.9	25.7	20.4	26.5	24.5	23.6	21.9	18.7	19.4	21.3	18.7	23.3	17.4	25.1	21.3	45.8
Ge	1.7	1.43	2.05	1.6	1.53	1.37	1.61	1.79	1.9	1.66	1.55	1.67	1.82	1.48	1.39	1.99	1.71	2.17
Hf	7.9	9.5	18.1	6.81	6	14	10.3	8.07	6.81	3.28	4.64	5.8	3.09	7.96	7.38	5.08	5.53	4.12
Mo	0.63	0.77	1.57	0.41	11.8	12.3	2.07	9.84	5.93	1.61	8.54	0.75	0.84	0.24	0.47	0.27	5.25	34.5
Nb	17.6	17.7	37.3	8.41	12.5	22.5	30.4	26.8	31	14.9	9.47	23.7	6.69	21	16.4	16.1	16.9	18
Ni				9.5	8.1	10	22.9	25.3	20.8	79.6	11.7	14.9	39.3				5.5	20.6
Pb	18.6	27.1	21.6	29.8	26.5	27.3	22.3	16.1	14.6	6.19	13.5	17.6	7.25	31.8	22.7	41.1	38.7	7.99
Rb	236	172	240	147	251	177	146	101	112	72.4	133	100.3	118	210	190	306	306	128
Sn	3.98	3.32	5.91	2.22	2.83	2.38	2.41	1.68	2.07	2.29	3.87	2.42	13.4	2.09	3.59	10	4.55	1.63
Sr	99.3	121	89.7	533	74	238	381	341	249	398	285	266	212	157	68.5	75.2	86.3	49.9
Ta	1.73	1.25	2.65	0.78	1.24	1.27	2.08	1.85	2.25	1.07	0.87	1.82	0.6	2.49	1.53	2.35	2.7	5.57
Th	40.5	22.2	85	17	33.6	30.2	13.2	9.11	8.17	2.84	14.2	17.4	10.6	35.5	37.1	33.1	33.7	25.5
U	5.57	2.25	6.78	2.59	4.16	3.98	2.79	3.34	1.76	0.63	2.19	2.6	1.81	5.55	4.86	6.46	7.88	7.38
V	10.1	22.7	26.6	33.9	16.8	37.4	106	119	127	1.57	154	86	172	15.3	8.1	3.7	10.4	31.3
W	1.12	0.8	0.65	0.28	11.6	12.5	1.55	8.89	4.67	2.19	9.2	3.93	5.62	0.56	1.04	1.37	5.84	34.8
Y	37.3	35.5	71.3	12.5	31.2	49.5	43.9	40.7	40.7	23.1	28.8	34.6	24.9	36.9	28.2	21.3	32	23.3
Zn	43.2	50.8	90.6	74.9	29.7	60.8	127	128	136	98.9	76.3	82.4	113	34.3	38.5	45.5	21.4	87.8
Zr	279	357	599	280	202	580	439	350	272	133	162	221	118	287	245	163	166	118
La	106	127	306	77.8	86.6	214	79.9	65.7	45.8	24.1	52.1	70	33	98.6	74.4	73.9	60.2	54.9
Ce	200	245	603	143	164	350	163	128	98.4	49.3	106	138	65.1	190	145	153	121	118
Pr	21.3	25.6	60.6	14.6	17	39.2	18.9	14.9	12.7	5.88	11.4	15	7.13	19.8	16.2	17.5	12.7	12.8
Nd	74.2	88.3	198	49.5	56.1	130	73.3	60.6	50	22.6	39.1	51.8	25.5	67.5	55.4	62.7	44.3	44.5
Sm	12.3	13.6	31	6.38	10.2	19.1	13.5	11.2	10.3	4.59	7.02	9.11	4.79	10.7	9.37	11.1	8.19	8.76
Eu	0.94	1.18	1.02	1.50	0.76	2.19	2.54	2.48	1.64	1.48	1.19	1.46	0.92	1.31	0.67	0.67	0.64	0.31
Gd	9.09	9.6	20.5	4.04	7.07	13.6	10.9	9.64	8.98	4.71	6.01	7.57	4.81	8.52	7.05	7.16	6.15	5.51
Tb	1.31	1.36	2.77	0.527	1.1	2.05	1.5	1.37	1.28	0.702	0.923	1.08	0.745	1.21	0.96	0.952	1.02	0.818

(*continued on next page*)

Table 3 (*continued*)

	Amphibole–biotite granite						MME			Dykes			Biotite syenogranite Orbicule				
	T3	T6	T11	T14	E4	E9	T8E	E4e1	E3-e1	E7e	S	T9	T13	T5	T4	T12	E1a	E1e
Dy	7.23	7.45	13.7	2.69	5.71	9.17	8.73	7.48	7.46	3.96	5.31	6.3	4.36	7.07	5.62	4.76	5.32	4.39
Ho	1.28	1.36	2.38	0.45	1.11	1.73	1.51	1.46	1.37	0.814	1.07	1.22	0.852	1.3	0.985	0.744	1.01	0.743
Er	3.53	3.42	6.42	1.17	2.92	4.78	3.94	3.82	3.96	2.16	2.88	3.23	2.3	3.53	2.76	1.9	3.06	2.01
Yb	3.28	3.23	5.74	1.15	2.64	4.15	3.87	3.47	3.75	2.13	2.64	3.24	2.43	3.67	2.69	1.79	3.08	1.86
Tm	0.55	0.51	0.94	0.17	0.47	0.75	0.60	0.62	0.62	0.34	0.40	0.50	0.36	0.55	0.44	0.27	0.48	0.34
Lu	0.48	0.46	0.88	0.17	0.38	0.59	0.59	0.52	0.56	0.33	0.44	0.45	0.36	0.53	0.39	0.27	0.42	0.28
A/CNK	1.03	1.01	1.03	1.04	1.03	0.98	0.85	0.84	0.75	0.70	0.81	0.89	0.70	1.06	1.03	1.12	3.35	1.11
ΣREE	441	528	1253	303	356	791	383	311	247	123	236	309	153	414	322	337	255	268
La_N/Yb_N	21.8	26.6	36.0	45.7	22.2	34.8	14.0	12.8	8.3	7.6	13.3	14.6	9.2	18.2	18.7	27.9	19.9	13.2
Dy_N/Lu_N	1.52	1.61	1.56	1.62	1.49	1.56	1.48	1.43	1.33	1.19	1.20	1.41	1.20	1.32	1.46	1.75	1.58	1.27
Eu/Eu*	0.26	0.30	0.12	0.84	0.26	0.40	0.62	0.71	0.51	0.96	0.55	0.52	0.58	0.41	0.24	0.21	0.13	0.27

7. Geochemistry

7.1. Analytical techniques

7.1.1. Major and trace elements

Seventeen representative samples (Table 3) of different granitic facies have been analyzed at the CRPG, Nancy, France using ICP-AES (major elements) and ICP-MS (trace elements). See the CRPG website for details. Major elements have been recalculated to 100 wt% on a water-free basis. The most important ratios discussed in the paper have been added in Table 3.

7.1.2. Sr–Nd isotopes

After acid dissolution of the sample in a beaker or in a pressure vessel if any solid was present after centrifugation, and Sr and Nd separation on ion-exchange resin, Sr isotopic compositions have been measured on Ta simple filament (VG Sector 54), Nd isotopic compositions on triple Ta–Re–Ta filament (VG Sector 54) in the Section of Isotope geology of the Africa Museum, Tervuren. Repeated measurements of Sr and Nd standards have shown that between-run error is better than 0.000015 (2σ). The NBS987 standard has given a value for $^{87}Sr/^{86}Sr$ of 0.710267 ± 0.000005 (2σ on the mean of 12 standards, normalised to $^{86}Sr/^{88}Sr = 0.1194$) and the Rennes Nd standard a value for $^{143}Nd/^{144}Nd$ of 0.511959 ± 0.000006 (2σ on the mean of 24 standards, normalised to $^{146}Nd/^{144}Nd = 0.7219$) during the course of this study. All measured ratios have been normalised to the recommended values of 0.710250 for NBS987 and 0.511963 for Nd Rennes standard (corresponding to a La Jolla value of 0.511858) based on the 4 standards measured on each turret together with 16 samples. Decay constant for ^{87}Rb (1.42×10^{-11} a^{-1}) was taken from Steiger and Jäger (1977) and for ^{147}Sm (6.54×10^{-12} a^{-1}) from Lugmair and Marti (1978). Results are given in Table 4.

7.2. Major and trace elements geochemistry

As a whole, the Temaguessine forms a monzonitic suite: MME and dykes are monzodiorite, quartz–monzodiorite and quartz–monzonite, the amphibole–biotite facies is both monzo- and syenogranitic while the biotite facies is only syenogranitic (Fig. 7A). The mafic and intermediate enclaves and dykes are metaluminous, the amphibole–biotite is moderately peraluminous and the biotite syenogranite slightly more peraluminous (Fig. 7B). The reference cordierite-bearing granites used for the biotite composition are much more peraluminous, having A/CNK ratios between 1.15 and 1.40 (Fig. 7B). By contrast, the cordierite-free Tarçouate pluton (Barbey et al., 2001) is comparable to Temaguessine. The slight peraluminous character of the Temaguessine pluton does not prevent it to be high-K calc-alkaline, alkali-calcic or even shoshonitic (Duchesne et al., 1998), the latter characteristic being shared by the Pilon pluton (Fig. 7C). Except the intermediate dykes,

Table 4
Sr and Nd isotopic ratios for the Temaguessine pluton

		Rb	Sr	$^{87}Rb/^{86}Sr$	$^{87}Sr/^{86}Sr$	2σ	Sri(582)	Sm	Nd	$^{147}Sm/^{144}Nd$	$^{143}Nd/^{144}Nd$	2σ	$\varepsilon_{Nd,582}$	TCHUR	TDM
Amp-bio gr	T3	236	99.3	6.920	0.770658	0.000009	0.71323	12.3	74.2	0.1002	0.511764	0.000007	−9.9	1379	1715
Amp-bio gr	T11	240	89.7	7.795	0.776358	0.000008	0.71167	31.0	198	0.0947	0.511740	0.000006	−9.9	1340	1666
Amp-bio gr	E4	251	74	9.893	0.787655	0.000009	0.70556	10.2	56.1	0.1099	0.511734	0.000007	−11.2	1585	1921
MME	E4e1	101	341	0.858	0.718204	0.000007	0.71108	11.2	60.6	0.1118	0.511772	0.000008	−10.6	1551	1898
MME	E7e	72	398	0.527	0.711558	0.000009	0.70719	4.59	22.6	0.1228	0.512061	0.000013	−5.8	1190	1642
Dykes	S	133	285	1.351	0.710239	0.000009	0.69903	7.02	39.1	0.1086	0.511890	0.000006	−8.0	1292	1668
Dykes	T9	100	266	1.093	0.719056	0.000007	0.70999	9.11	51.8	0.1064	0.511880	0.000008	−8.1	1277	1648
Bio gr	T5	210	157	3.884	0.742370	0.000007	0.71014	10.7	67.5	0.0959	0.511739	0.000010	−10.0	1357	1684
Bio gr	T4	190	68.5	8.081	0.777012	0.000013	0.70995	9.37	55.4	0.1023	0.511770	0.000008	−9.9	1399	1738
Bio gr	E1a	306	86.3	10.345	0.790782	0.000008	0.70493	8.19	44.3	0.1118	0.511820	0.000008	−9.7	1466	1826

the Temaguessine pluton is mostly ferriferous, by contrast with the other cordierite plutons (Fig. 7D). The cordierite-rich dark centre of an orbicule is characterized by a high quartz content (Fig. 7A), a very high A/CNK value (3.35, Fig. 7B), a low K_2O content (Fig. 7C) and a strong ferriferous character (Fig. 7D), in agreement with the abundant presence of Fe-cordierite.

The different facies of the Temaguessine plutons display similar REE patterns and spidergrams, taking into account their different silica contents (Fig. 8A–C). The Temaguessine biotite granite (Fig. 8A) is moderately enriched in REE and fractionated, with rather flat HREE and a pronounced negative Eu anomaly. It is remarkable that the REE pattern of the cordierite dark centre of the analyzed orbicule is similar to the biotite granite, the differences being a less important enrichment in REE and a deeper Eu negative anomaly. Three amphibole–biotite granite samples (Fig. 8B) are similar to the biotite granite; two other samples are strongly more enriched. Sample T14 is strongly different and looks very much like the REE pattern of the Anfeg batholith (Acef et al., 2003). This sample is thus most likely a xenolith from the nearby Azrou n'Fad batholith (Fig. 2). Except sample E7e, the MME and dykes (Fig. 8C), display similar REE patterns: mildly enriched in REE, slightly enriched in LREE, rather flat HREE and a negative Eu anomaly. Sample E7e has nearly no Eu anomaly but does not have the high La/Yb ratio of the Azrou n'Fad xenolith T14. All spectra share a common signature: (high REE content and La_N/Yb_N in the 10–40 range), which likely point to a cogenetic origin and evolution.

The N-MORB-normalized spidergrams of Temaguessine granitoids (Fig. 8D, E) show remarkably similar patterns. They display an enrichment in LILE and negative anomalies in Ba, Nb, Ti and P; in a normal magmatic differentiation process, the negative anomaly observed for Sr, Ba, P and Ti can be ascribed to the fractionation of plagioclase, K–feldspar, apatite and ilmenite and/or titanite, respectively.

The mafic microgranular enclaves and dykes (Fig. 8F) have patterns roughly similar to those of the granites but they are slightly more enriched in LILE and present a weak negative anomaly in P and Ti.

The trace elements patterns in the Temaguessine granites are comparable to the Silet Taourirt 'GIII' (Azzouni-Sekkal et al., 2003) composition (Fig. 8G, H). The Temaguessine pluton is more enriched than the Taourirt GI and than the Anfeg batholith, which has particularly low HREE (cf. the attribution of sample T14 to the Azrou n'Fad batholith). The Taourirt magmatic province represents the youngest post-collisional igneous event in the Tuareg shield (530–525 Ma; Cheilletz et al., 1992; Fig. 1B).

7.3. Sr–Nd isotopes

The Sr and Nd isotopic ratios have been calculated back to 582 Ma, the crystallization age (U–Pb zircon) of the Temaguessine pluton.

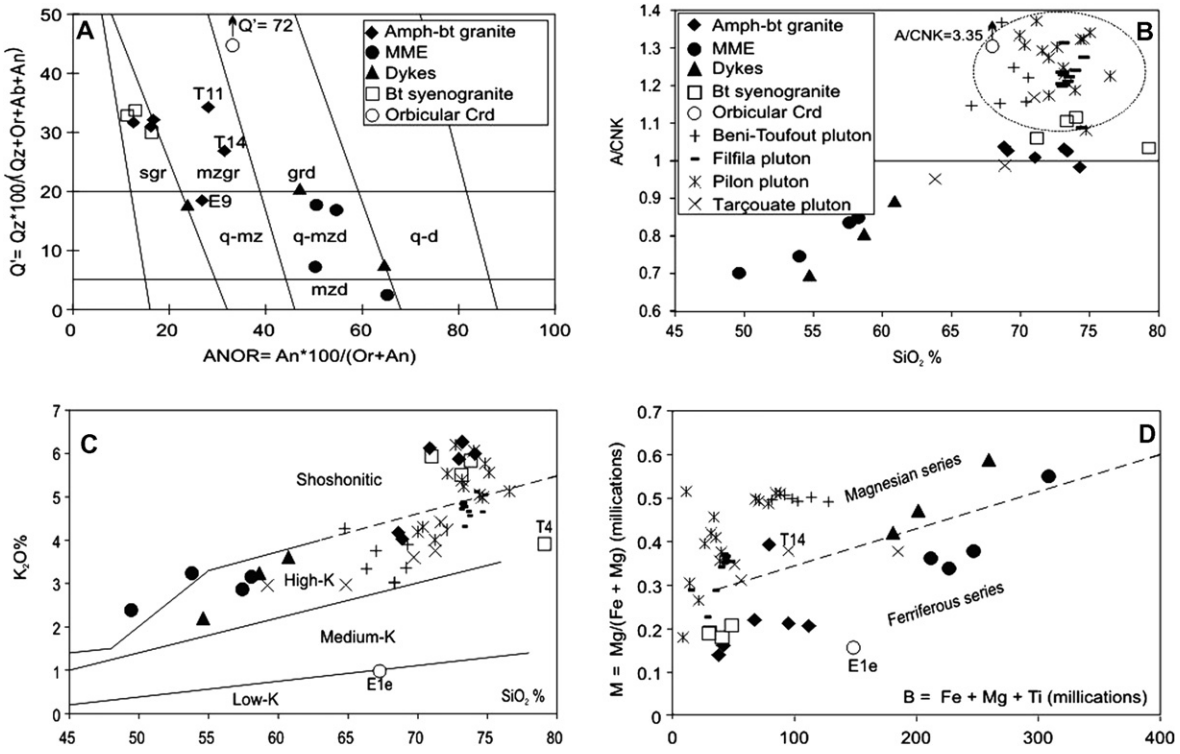

Fig. 7. Main geochemical characteristics of the Temaguessine granitoids. (A) Normative classification in the Q'–ANOR diagram (Streckeisen and Le Maitre, 1979); (B) SiO_2 vs. A/CNK (molar $Al_2O_3/CaO + Na_2O + K_2O$) of the Temaguessine pluton compared to the Tarçouate pluton and cordierite-bearing granitoids; (C) SiO_2 vs. K_2O (subdivisions from Rickwood, 1989) of the Temaguessine pluton compared to the Tarçouate pluton and cordierite-bearing granitoids; (D) Ferrous character of the Temaguessine granitoids (fields after Debon and Lefort, 1988) compared to the more magnesian Tarçouate pluton and cordierite-bearing granitoids.

The biotite–amphibole granite and the biotite syenogranite show the same variation in Nd and Sr initial isotopic ratios (Table 4): ε_{Nd} values vary between −9.9 and −11.2 and between −9.7 and −10 and I_{Sr} values vary between 0.705 and 0.713 and 0.704 to 0.710, respectively. The microgranular enclaves have ε_{Nd} values ranging from −5.6 to −10.6 and I_{Sr} values from 0.707 to 0.711. ε_{Nd} and I_{Sr} of the dykes are −8 and 0.709 respectively. It must be noted that an errorchron can be calculated with 7 samples (excluding the dyke and one MME): 559 ± 44 Ma, $I_{Sr} = 0.7116 \pm 0.0042$, MSWD = 7.7. Within error limits (quite large here) this age is identical to the zircon age (582 ± 5 Ma) implying that the obtained I_{Sr} (0.707–0.716) encompasses most of the initial variability in Sr isotopes of the Temaguessine pluton. The two lower I_{Sr} of the granites E1a (0.7049) and E4 (0.7056) cannot be considered to indicate a more juvenile batch due to their high Rb/Sr ratio (around 10, inducing a high uncertainty on their individual I_{Sr}); the I_{Sr} of dyke S (0.6990), which has a moderate Rb/Sr ratio (around 1) is too low and indicates a later perturbation that may be due to alteration. This is confirmed by the ε_{Nd} of this sample, close to the value of the other dyke T9.

8. Genesis of the orbicular Fe-cordierite from the Temaguessine pluton

The occurrence of cordierite in granitoids should be interpreted according to petrographical observations since chemical discrimination is often impractical. In his compilation, Clarke (1995) petrographically defined three types of cordierites, each having a different origin: the type 1 corresponds to inherited cordierite (xenocrystic or restitic) near the host country rocks or within xenoliths. This is the case of the Alpine cordierite-bearing granites of northern Algeria (Ouabadi, 1994; Fourcade et al., 2001). The type 2 corresponds to magmatic cordierite crystallizing either directly from the silicate magma or from a reaction between the magma and a pre-existing mineral. In this case, the cordierite crystal is often euhedral and inclusion-free. The type 3 is late metasomatic cordierite in equilibrium with a water-rich fluid phase. The cordierite crystals are often associated with quartz and show graphical texture.

Orbicular cordieritites (Gordillo, 1979; Schreyer et al., 1979) in granitic rocks are very scarce. They were first reported by Mathias (1952) in the Upington granite, South Africa and are composed of 63% porphyric cordierite. Such cordieritites are now well known in peraluminous (leuco)granites, e.g. those of the Central Iberian Massif (Ugidos, 1988).

In the Temaguessine biotite syenogranite, the Fe-cordierite orbicules are unusually large spherical enclaves (10–20 cm in diameter). They are distributed over a surface of a few hundred square metres around a 100-m-long quartzite xenolith. The occurrence of the orbicules within the granite resembles the massive and orbicular cordieritites of the El Pilon granite, Argentina (Rapela et al., 2002). However,

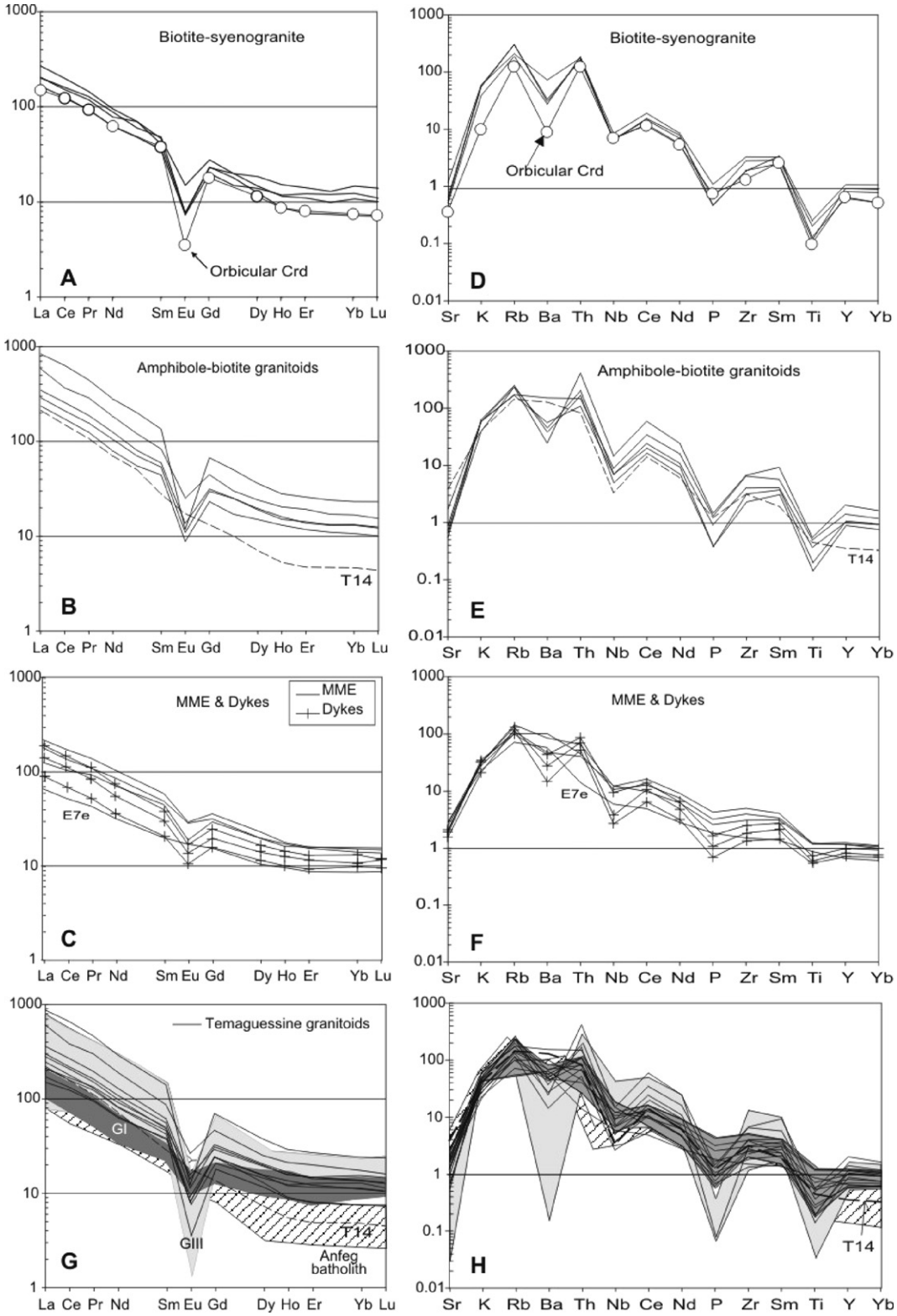

Fig. 8. REE diagrams (A–C, G; normalization to chondrite; Taylor and McLennan, 1980) and spidergrams (D–F, H; normalised to MORB; Sun, 1980; Pearce, 1982) of the Temaguessine granitoids and reference Anfeg and Taourirt plutons (G, H); (A) REE patterns for the biotite syenogranite and the orbicular cordierite; (B) REE patterns for the biotite amphibole–biotite granite; (C) REE patterns for the mafic microgranular enclaves (MME) and dykes; (D) spidergram for the biotite syenogranite; (E) spidergram for the amphibole–biotite granite; (F) spidergram for the mafic microgranular enclaves (MME) and dykes; (G) comparison of the REE patterns of the granites of the Temaguessine pluton, the Taourirt GI and GIII groups (Azzouni-Sekkal et al., 2003) and the Anfeg Batholith (Acef et al., 2003); and (H) as in G, but spidergram. T14 is a xenolith from the nearby Azrou n'Fad batholith.

several differences between the El Pilon and the Temaguessine granites emerge: (1) the El Pilon granite is strongly peraluminous whereas the Temaguessine granite is moderately peraluminous; (2) in the El Pilon granite, the cordierite orbicules are egg-shaped (10–30 cm), show a cumulate aspect and are surrounded by a corona that is composed of biotite + sillimanite. In the Temaguessine biotite syenogranite, the orbicules are spherical with a corona composed of quartz and feldspar and no sign of cumulate is observed. (3) The cordieritites of the El Pilon granite are composed of cordierite + biotite + sillimanite while those of Temaguessine comprise cordierite, quartz and scarce phantoms of Fe–biotite flakes largely transformed into Fe-cordierite.

The Temaguessine cordierite is not of type 3 (metasomatic) as it is included in an orbicule itself in the granite where no trace of fluid activity is recorded. It is not of magmatic origin as it is clearly in disequilibrium with the granitic magma (quartz–feldspar rim). It is not restitic as no expected high-grade minerals are present. It cannot be a true xenocryst as the cordierite known in the country-rocks is Mg-rich (Guiraud et al., 1996) and not Fe-rich as in the Temaguessine orbicules (Fig. 4E).

The only solution is to consider that the Temaguessine cordierite crystallized inside a xenolith within the granitic magma. This is sustained by (1) the reaction rim around the cordieritites; (2) destabilised Fe–biotite inclusions in cordierite, now only seen as ghosts; both observations suggesting an important recrystallization within the orbicule; (3) the Temaguessine granite is not peraluminous enough to generate the cordierite; and (4) the presence of a mega-xenolith of quartzite (Fig. 3C) suggests that the roof of the pluton collapsed into the magma, rendering the presence of numerous smaller xenoliths of all size in the vicinity very likely, particularly if the exploding xenolith model of Clarke et al. (1998) is taken into account. As we did not find gneissic xenoliths in the vicinity of the orbicules, this means that the explosion process achieved completion. With this model, three questions arise: what are the reactions and the P–T conditions at the origin of the cordierite? What is the origin of the felsic rim? What was the nature of the protolith of the xenolith?

The biotite ghosts suggest that the formation of cordierite is related to the dehydration–melting of biotite according, as mentioned in the Velay anatectic massif (Dupraz

Table 5
Calculations from the chemistry of the cordierite orbicule

A. Calculation of the mineral composition of a cordierite orbicule from the chemistry

	Qtz	An29 Plag	Or	Bt	Crd	calculated assemblage	Crd orbicule	Difference
Ech		T12-33	T12-36	T12e	E1e		E1e	
SiO2	100.00	61.55	65.10	34.73	44.66	***67.34***	**67.95**	-0.61
TiO2			0.03	3.69	0.05	***0.35***	**0.14**	0.21
Al2O3		24.99	18.47	18.59	28.69	***16.10***	**15.81**	0.29
FeOt		0.13	0.08	23.97	17.79	***9.36***	**9.76**	-0.40
MnO			0.05	0.32	0.91	***0.40***	**0.45**	-0.05
MgO				3.27	1.54	***0.92***	**0.94**	-0.02
CaO		5.96	0.04	0.05	0.23	***0.73***	**0.74**	-0.01
Na2O		7.89	0.40	0.17	1.37	***1.41***	**1.38**	0.03
K2O		0.38	16.14	9.14	0.07	***1.05***	**1.02**	0.03
% phase	**39.0**	**10.6**	**1.0**	**9.0**	**40.4**			
Q'					Q'	77.08		

B. Calculation of the chemical composition of the protolith of the cordierite orbicule

	Crd orbicule *assemblage*	leucocratic rim An19 Qtz	Plag	Or	calculated assemblage		
Minimum 3 kbar		30	47	23		**CIPW norm**	
SiO2	***67.95***	100.00	63.82	65.10	***72.02***	Qz	40.13
TiO2	***0.14***			0.03	***0.06***	Co	6.90
Al2O3	***15.81***		24.41	18.47	***15.76***	Or	16.33
FeOt	***9.76***		0.13	0.08	***4.15***	Pl	31.98
MnO	***0.45***		0.09	0.05	***0.22***	PlAn	5.59
MgO	***0.94***		0.00		***0.39***	PlAb	26.39
CaO	***0.74***		3.55	0.04	***1.28***	Hy	1.11
Na2O	***1.38***		8.18	0.40	***2.86***	Mt	1.95
K2O	***1.02***		0.40	16.14	***2.69***	Il	0.09
% phase	**42.0**	**17.4**	**27.3**	**13.3**		Hm	1.21
A/CNK					**1.58**	Ap	0.30
Q'					**45.4**		
ANOR					**25.5**	***= (grey)wacke***	

An orbicule 10 cm in diameter with a leucocratic rim of 1.25 cm is made, in volume, of 42% of the central cordierite-rich core and of 58% of the leucocratic rim

and Didier, 1988), to the reaction biotite + plagioclase + Al_2O_5 = $KAlSi_3O_8$ + cordierite + melt ($P < 0.4$ GPa and $T° < 850$ °C; Le Breton and Thompson, 1988). These P–T conditions are compatible with the Temaguessine pluton. The reaction, which is an incongruent melting, implies a peraluminous protolith and produces a melt, which could then form the leucocratic rim. We suggest that in the case of the Temaguessine pluton, the melt is expulsed from the partially molten xenolith by filter pressing due to the magma pressure. A simple mass balance calculation shows that this model is tenable (Table 5). First, using the composition of the cordierite from the centre of the orbicule (sample E1e) and the composition of plagioclase, K–feldspar and biotite from sample T12, it is possible to build a mineralogical assemblage (40% cordierite, 39% quartz, 11% plagioclase, 9% biotite and 1% K–feldspar) in agreement with the rough mode of the orbicule. This demonstrates the validity of the chemical analysis. Second, this analysis can be used to build the chemical analysis of the protolith by adding the correct proportion of a quartz–feldspar melt corresponding to the felsic rim. We took here, as an approximation, the composition of a minimum melt at 0.3 GPa (30% quartz, 47% plagioclase (An_{19}), 23% K–feldspar). Taking an orbicule of 10 cm in diameter with a leucocratic rim of 1.25 cm, this implies, in volume, 42% of the cordierite-rich core and 58% of the leucocratic rim. With these proportions, the calculated assemblage has (normative) 40% quartz, 32% plagioclase, 16% K–feldspar, 7% corundum and a few percent of other minerals (Table 5). This is equivalent to a composition of a peraluminous greywacke.

We can thus propose (Fig. 11) that the Temaguessine cordierite orbicule resulted from the collapse of a wacke into the granitic magma at a temperature of about 800 °C and at a pressure of c. 0.3 GPa, which induced its incongruent melting and in turn induced (1) the expulsion of the felsic melt produced by the magma overpressure which crystallized around the unmelted part of the xenolith, forming the felsic rim and (2) the solid product of the incongruent melting of the xenolith became highly peraluminous (A/CNK = 3.35), with abundant cordierite (40%) which is Fe-rich (Fe# = 0.87) due to the fact that, in the orbicule, all the iron of the protolith (4%; Table 5) is concentrated in the cordierite.

We must, however, consider the fact that the biotite from the biotite syenogranite is also rich in iron (Fig. 4A)

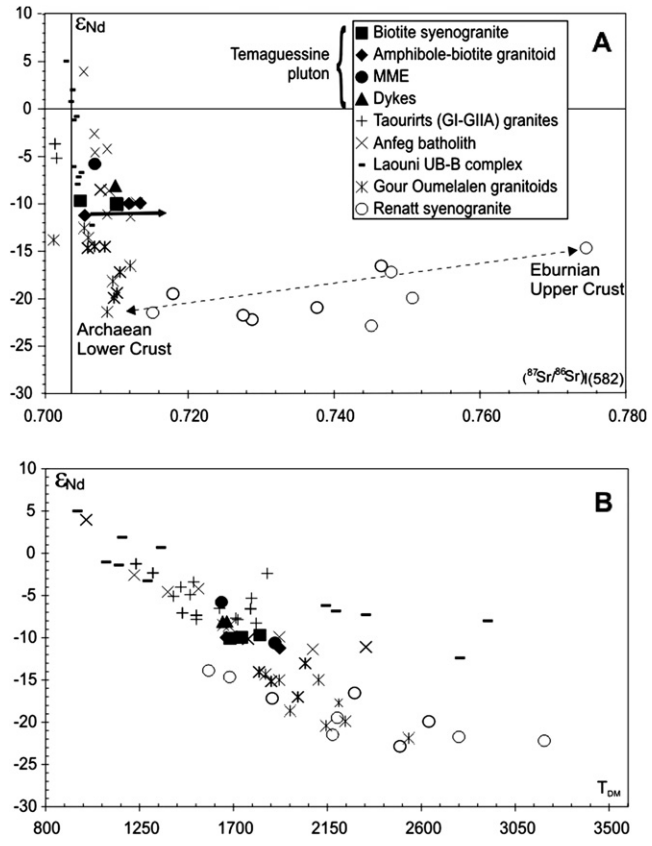

Fig. 9. Sr and Nd isotopic data for the Temaguessine granites and for other granites from the Tuareg shield: Taourirt granites (Azzouni-Sekkal et al., 2003), Anfeg batholith (Acef et al., 2003), Laouni ultrabasic-basic (UB-B) complex (Cottin et al., 1998), Gour Oumelalen granitoids (Liégeois et al., 2003) and Renatt syenogranite (Liégeois et al., 1994). (A) $\varepsilon_{Nd(582Ma)}$ vs. $(^{87}Sr/^{86}Sr)_{i(582Ma)}$; (B) $\varepsilon_{Nd(582Ma)}$ vs. Nd T_{DM} model ages.

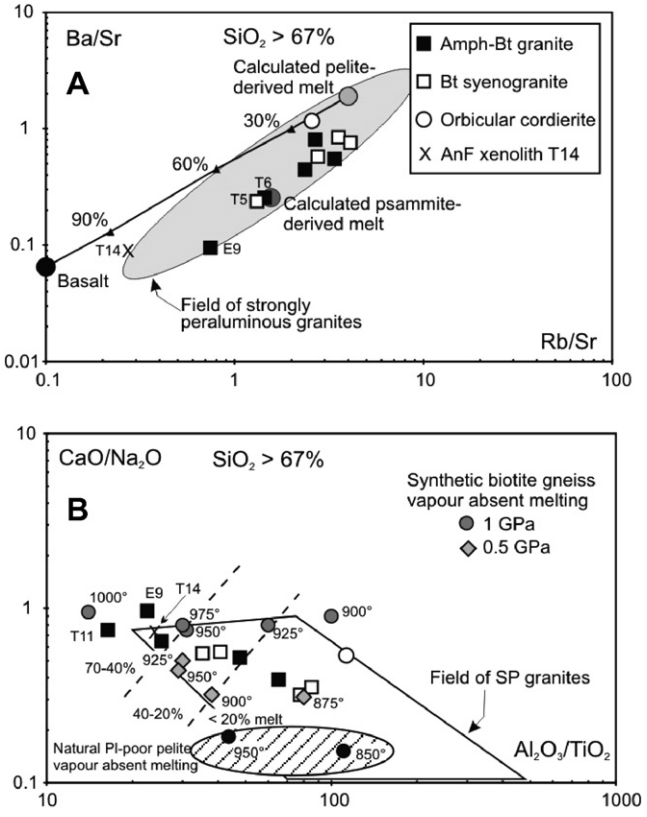

Fig. 10. (A) Ba/Sr vs. Rb/Sr diagram (Sylvester, 1998) showing that most of the Temaguessine granites are located between calculated psammite and pelite-derived melts; two samples plot in direction of the basalt composition. AnF = Azrou n'Fad. (B) CaO/Na_2O vs. Al_2O_3/TiO_2 (Sylvester, 1998) showing that the Temaguessine granites plot between the 0.5 and 1 GPa trends at temperatures between 900 and 980 °C, at a distance from the field of the natural plagioclase (pl)-poor pelite vapour absent melting. Same legend as in A.

and in alumina (Fig. 4A, C). This can be explained by two opposite possibilities: (1) the complete assimilation of smaller xenoliths similar in composition to the Fe-wacke at the origin of the orbicules adds iron which is incorporated within the biotite; (2) the Fe–biotite crystallized only from the granitic magma itself enriched in iron and some mixing occurred between the granitic magma and the melt generated in the xenoliths; the iron which is not incorporated in the quartz–feldspar melt is integrated in the crystallizing cordierite. There are no definite arguments in favour of one or other of these models, but taking into account the sharp contact between the granite and the leucocratic rim around the orbicules, we favour the first interpretation.

9. Genesis of the Temaguessine magma

The similarity of the geochemistry (Fig. 8) of all the Temaguessine facies (amphibole–biotite granite, biotite syenogranite, MME, dykes) indicates that they share a common history. The Temaguessine Sr–Nd isotopic ratios ($I_{Sr} = 0.704$–0.710 and ε_{Nd} between -9.6 and -11.2) display a variation that can be interpreted as a variable incorporation of a material coming from an Eburnian upper crust. When compared to other granites from LATEA, most of the Temaguessine granites Sr–Nd isotopic initial ratios are located at the lower end of the Anfeg batholith, i.e. with relatively radiogenic Sr for a given ε_{Nd} (Fig. 9A); two samples are located more to the left at the lower end of the Laouni basic-ultrabasic trend (Cottin et al., 1998), close to the upper end of the Gour Oumelalen granitoids (Liégeois et al., 2003). The main Temaguessine trend indicates that the crustal pole in its genesis corresponds to a relatively enriched (Rb undepleted) continental crust known to be the source of an end-member of the Renatt granite (Liégeois et al., 1994, 1998; Fig. 9A). The inherited zircons dated suggest that this continental crust is Eburnian in age

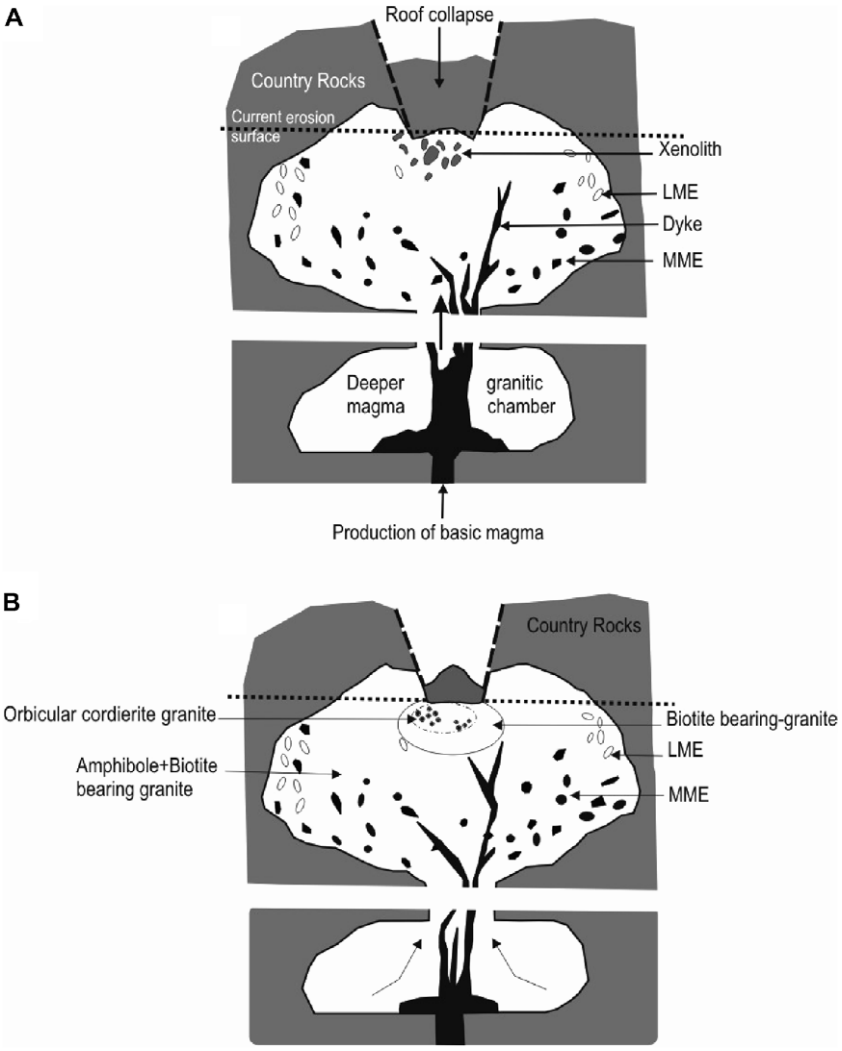

Fig. 11. Genesis of the Temaguessine pluton and of the cordierite orbicules. (A) In a deep magma chamber (0.7–0.8 GPa), intrusion of basic magma from the mantle induces the partial melting of the continental crust. The two magmas moves upward and partly mingle, forming the MME and the mafic dykes; light microgranular enclaves (LME) represent marginal facies detached from the contact with the country-rocks; blocks and particles of all sizes from the country-rock roof collapse into the magma. (B) The gneissic xenoliths are affected by partial melting and recrystallization due to the high temperature (>900 °C) and the pressure (c. 0.3 GPa), some of them being transformed in cordierite orbicules.

(c. 2 Ga). Nd T_{DM} model ages of all samples vary from 1.64 to 1.92 Ga (Fig. 9B), at the lower end of both the Anfeg batholith and Taourirt plutons T_{DM} bracket. These parameters point to a large participation of the Eburnian continental crust in the genesis of the Temaguessine pluton but also to some participation of mantle (asthenospheric) material.

The high K_2O content points to a pelite or psammitic-derived melt composition: this is shown in the Ba/Sr vs. Rb/Sr diagram (Fig. 10A; Sylvester, 1998). Although most Temaguessine granites are moderately peraluminous, they do plot in the strongly peraluminous field (A/CNK > 1.10) compiled by Sylvester (1998). Most Temaguessine granites fall between the calculated pelite- and psammite-derived melts (Sylvester, 1998 and references therein); two granites correspond to the calculated psammite-derived melt (T5 and T6) and one (E9) requires the addition of a basaltic component; the orbicule cordierite-rich core is close to the calculated pelite-derived melt. It must be noted that the two samples T5 and T6 are two samples close to the quartzite xenolith (Fig. 2): their distinct composition could be influenced by the collapse and explosion of the xenoliths, determined to be a wacke (geochemically similar to a psammite) on the basis of the orbicules (see above). Azrou n'Fad xenolith T14 is rather different and is not considered here. The use of the Al_2O_3/TiO_2 ratio allows the estimation of the temperature of the melting and, combined to the CaO/Na_2O ratio, to roughly evaluate the pressure and/or the psammite/pelite ratio (Sylvester, 1998 and reference therein). Indeed, during melting of a given pelitic or psammitic source, the Al_2O_3 will remain constant during the increase in temperature due to stability of the aluminous refractory phase; while, in contrast, the TiO_2 will increase with temperature due to the progressive break-down of Ti-rich phases such as biotite and ilmenite. On the other hand the CaO/Na_2O ratio will be higher in psammite-derived melts than in pelite-derived melt and higher at higher pressure (Fig. 10B). The Temaguessine granites determine a trend corresponding to a psammite (biotite gneiss)-derived melt between 875 and 980 °C at a pressure of 0.7–0.8 GPa. The highest temperature (sample E9) is linked to a larger basaltic component, as it seems to be the case for the Azrou n'Fad xenolith (T14). The peculiar position of sample T11 is due to a very low Al_2O_3 content (12.8%), which is currently not understood.

Considering the composition of the source (lower continental crust with some asthenospheric mantle participation) and the position of the Temaguessine pluton along a major shear zone of the Azrou n'Fad terrane, we adopt here the model proposed for the LATEA batholiths and high-level plutons by Acef et al. (2003) and Liégeois et al. (2003) that these intrusions are linked to a linear lithospheric delamination along mega-shear zones, allowing the hot asthenosphere to rise, melt by adiabatic pressure release, inducing the melting of the Palaeoproterozoic lower crust.

10. Geodynamical implications of the Temaguessine pluton

The Temaguessine pluton is a high-level subcircular pluton. Its well-constrained age of 582 ± 5 Ma implies that the LATEA metacraton was at this time already uplifted from the depth needed for the batholiths, such as the Anfeg batholith (0.5 GPa; c. 615 Ma; Bertrand et al., 1986; Acef et al., 2003). It implies also that the degree of partial melting of the lower crust at c. 580 Ma was much less, the volume of the Temaguessine pluton and similar plutons being very low. We can thus consider that the Temaguessine pluton, together with other late subcircular plutons such as the Tihodaine (Abdallah et al., 2003) and Tisselliline plutons (NE Central Hoggar; Rb–Sr age of c. 555 Ma; Liégeois et al., 2003) are marking the end of the Pan-African orogeny in the LATEA metacraton as it is considered to be the case for the Iforas alkaline–peralkaline province dated by the Rb–Sr method in the 560–540 Ma age range (Boullier et al., 1986; Liégeois and Black, 1987; Liégeois et al., 1996). We must note that there is a strong need for U–Pb zircon ages for these late occurrences that could be slightly older than the Rb–Sr ages and thus could be contemporaneous to the Temaguessine pluton.

This means that the younger Taourirt plutons (535–525 Ma; Azzouni-Sekkal et al., 2003 and references therein) precisely dated by the U–Pb zircon method (Tioueine pluton at 524 ± 1 Ma; Paquette et al., 1998) occurred after the end of the Pan-African orogeny within the Tuareg shield and should not be considered as a very late-Pan-African event (Azzouni-Sekkal et al., 2003) but as an anorogenic Cambrian magmatic event. This is not in contradiction with the observation that the Taourirt plutons such as the Tioueine pluton are contemporaneous to a tectonic phase and then considered as syn-tectonic (Djouadi et al., 1997; Paquette et al., 1998): anorogenic magmatism is always accompanied by a tectonic reactivation of older structures (e.g. Devonian Aïr ring complexes, Moreau et al., 1994; Cenozoic Hoggar volcanism, Liégeois et al., 2005; alkaline magmatism as a whole, Black and Liégeois, 1993; Bonin et al., 1998). It must be noted that the model proposed for the generation of the Taourirt province by Azzouni-Sekkal et al. (2003), a tectonic response to far-distance stress at plate margins, fits with our conclusion.

11. Conclusions

The Temaguessine subcircular pluton in Central Hoggar (LATEA metacraton) is remarkable by the presence of Fe-cordierite orbicules particularly in a moderately peraluminous potassic magma. Also, its geotectonic position gives to this pluton a major status as a marker in the evolution of the Pan-African orogeny in the Tuareg shield. We can conclude:

(1) The Temaguessine pluton is a high-level elliptical intrusion. It is an alkali-calcic pluton composed of amphibole–biotite granite and biotite syenogranite

including mafic microgranular enclaves (quartz monzodiorite), country-rock xenoliths and cordierite-rich orbicules. It is intrusive along a NW–SE major shear zone, within the Azrou n'Fad terrane composed of Eburnian (c. 2 Ga) gneisses and of Pan-African (c. 615 Ma) granitic batholiths.

(2) The cordierite orbicules are composed of a cordierite-rich core (40%) and a leucocratic rim. They are located in the centre of the pluton near a 100-m-long quartzite xenolith, in a place where the roof of the pluton collapsed into the granitic magma. The cordierite orbicules resulted from the incongruent melting of meta-wacke xenoliths that have fallen in the magma. The resulting quartz–feldspar minimum melt obtained through dehydration melting of the biotite was extracted by overpressure and formed the leucocratic rim. The solid product of the incongruent melting was highly peraluminous (A/CNK= 3.35), with a high proportion of cordierite. The orbicule generation occurred at $T < 850°$ and $P < 0.3$ GPa.

(3) The Temaguessine cordierite is particularly rich in iron (Fe# = 0.87). This is probably the consequence of a Fe-rich protolith (wacke with 4% Fe_2O_3 for 72% SiO_2). However, it is not sure if the Fe-rich and Al-rich composition of the biotite in the biotite syenogranite, enclosing the cordierite orbicules, is a consequence of the process (complete assimilation of smaller xenoliths) or implies some mixing between the granitic magma and the melt generated in the xenoliths. However, taking into account the leucocratic rim around the orbicules, we privilege the first interpretation.

(4) The Temaguessine pluton is dated (SHRIMP U–Pb on zircon) at 582 ± 5 Ma. Inherited zircons have been dated at c. 610 Ma (Pan-African batholith), 1.76, 1.87 and 2.04 Ga (Hoggar Palaeoproterozoic basement).

(5) The different Temaguessine magmatic facies (amphibole–biotite granite, biotite syenogranite, MME, dykes) have a similar geochemistry (Fig. 8) suggesting a common magmatic history. Strongly negative ε_{Nd} between −9.6 and −11.2, Nd T_{DM} model ages between 1.64 to 1.92 Ga, inherited zircons between 1.76 and 2.04 Ga and variable I_{Sr} (0.704–0.710) demonstrate that this source is the Rb-depleted lower continental crust of the Azrou n'Fad terrane, part of the Palaeoproterozoic LATEA metacraton mixed with some mantle material for explaining the existing, although short, isotopic trend. Such a mixing and thus a mantle contribution is confirmed when considering the available isotopic signature of the LATEA lower crust, which has more negative ε_{Nd} and higher I_{Sr} than the Temaguessine pluton.

(6) The Temaguessine pluton, together with other high-level subcircular plutons, is considered as marking the end of the Pan-African magma generation in the LATEA metacraton, resulting from the linear delamination along a mega-shear zone, allowing asthenospheric uprise and melting of the lower continental crust. The younger Taourirt granitic province (535–525 Ma) should be considered as a Cambrian anorogenic event unrelated to the Pan-African orogenic event in the region.

Acknowledgements

This is Tectonics Special Research Centre Publication number 419. We thank Bernard Bonin and Jean-Louis Paquette for their careful reviews that enhanced the quality and the impact of this article.

References

Abdelsalam, M., Liégeois, J.P., Stern, R.J., 2002. The Saharan metacraton. Journal of African Earth Science 34, 119–136.

Abdallah, N., Ouabadi, A., Fezaa, N., 2003. Geochemistry and tectonic setting of the Pan-African granite of Tihodaine (Egéré-Aleksod Terrane, central Hoggar, Algeria). Third International Symposium on Geophysics (ISG3), Tanta, Egypt, 14–16 October.

Acef, K., Liégeois, J.P., Ouabadi, A., Latouche, L., 2003. The Anfeg post-collisional Pan-African high-K calc-alkaline batholith (Hoggar, Algeria), emplaced within the LATEA metacraton. Journal of African Earth Science 37, 295–311.

Azzouni-Sekkal, A., Liégeois, J.P., Bechiri-Benmerzouk, F., Belaidi-Zinet, S., Bonin, B., 2003. The "Taourirts" magmatic province, a marker of the closing stage of the Pan-African orogeny in the Tuareg Shield: review of available data and Sr–Nd isotope evidence. Journal of African Earth Science 37, 331–350.

Barbey, P., Nachit, H., Pons, J., 2001. Magma–host interactions during differentiation and emplacement of a shallow-level, zoned granitic pluton (Tarçouate pluton, Morocco): implications for magma emplacement. Lithos 58, 125–143.

Barbey, P., Marignac, C., Montel, J.M., Macaudière, J., Gasquet, D., Jabbori, J., 1999. Cordierite growth textures and the conditions of genesis and emplacement of crustal granitic magmas: the Velay granite complex (Massif Central, France). Journal of Petrology 40, 1425–1441.

Bendaoud, A., Ouzegane, K., Kienast, J.R., 2003. Textures and phase relationships in ferrous granulites from Tidjenouine (Hoggar, Algeria): fayalite–ferrossilite–quartz secondary assemblage. Journal of African Earth Science 37, 241–255.

Bertrand, J.M.L., Caby, R., 1977. Carte géologique du Hoggar, Algeria. Direction des Mines et de la Géologie, SONAREM, scale 1:1000000, 2 sheets.

Bertrand, J.M., Michard, A., Boullier, A.M., Dautel, D., 1986. Structure and U/Pb geochronology of Central Hoggar (Algeria): a reappraisal of its Pan-African evolution. Tectonics 5, 955–972.

Beuf, S., Biju-Duval, B., De Charpal, O., Rognon, P., Gariel, O., Bennacef, A., 1971. Les grès du Paléozoïque inférieur au Sahara, Publication IFP, Collection "Science et techniques du pétrole, Paris 464pp.

Birch, W.D., Gleadow, A.J.W., 1974. The genesis of garnet and cordierite in acid volcanic rocks: evidence from the Cerberean cauldron, central Victoria, Australia. Contributions to Mineralogy and Petrology 45, 1–13.

Black, L.P., Kamo, S.L., Allen, C.M., Davis, D.W., Aleinikoff, J.N., Valley, J.W., Mundil, R., Campbell, I.H., Korsch, R.J., Williams, I.S., Foudoulis, C., 2004. Improved $^{206}Pb/^{238}U$ microprobe geochronology by the monitoring of a trace-element-related matrix effect; SHRIMP, ID–TIMS, ELA–ICP–MS and oxygen isotope documentation for a series of zircon standards. Chemical Geology 205, 115–140.

Black, B., Latouche, J.L., Liégeois, J.P., Caby, R., Bertrand, J.M., 1994. Pan-African displaced terranes in the Tuareg shield (central Sahara). Geology 22, 641–644.

Boissonnas, J., 1973. Les granites à structures concentriques et quelques autres granites tardifs de la chaîne panafricaine (sahara central, Algérie). Thèse, Centre de Recherche sur les zones Arides, Série Géologie 16, 662pp.

Black, R., Liégeois, J.P., 1993. Cratons, mobile belts, alkaline rocks and continental lithospheric mantle: the Pan-African testimony. Journal of the Geological Society of London 150, 89–98.

Bonin, B., Azzouni-Sekkal, A., Bussy, B., Ferrag, S., 1998. Alkali-calcic and alkaline post-orogenic (PO) granite magmatism: petrologic constraint and geodynamic settings. Lithos 45, 45–70.

Boullier, A.M., Liégeois, J.P., Black, R., Fabre, J., Sauvage, M., Bertrand, J.M., 1986. Late Pan-African tectonics marking the transition from subduction-related calc-alkaline magmatism to within-plate alkaline granitoids (Adrar des Iforas, Mali). Tectonophysics 132, 233–246.

Briedj, M., 1993. Étude géologique de la région de Tahifet (Hoggar central, Algérie). Implication géodynamique: thèse de Doctorat d'État, Université de Nancy I, France 189p.

Caby, R., 2003. Terrane assembly and geodynamic evolution of central-western Hoggar: a synthesis. Journal of African Earth Science 37, 133–159.

Caby, R., Andreopoulos-Renaud, U., 1983. Age à 1800 Ma du magmatisme sub-alcalin associé aux métasédiments monocycliques de la chaîne pan-africaine du Sahara central. Journal of African Earth Sciences 1, 193–197.

Cheilletz, A., Bertrand, J.M., Charoy, B., Moulahoum, O., Bouabasa, L., Farrar, E., Zimmerman, J.L., Dautel, D., Archibald, D.A., Boullier, A.M., 1992. Géochimie et geochronology Rb–Sr, K–Ar et ^{39}Ar-^{40}Ar des complexes granitiques pan-africains de la région de Tamanrasset (Algérie): relations avec les minéralisations Sn–W associées et l'évolution tectonique du Hoggar central. Bulletin de la Société Géologique de France 163, 733–750.

Clarke, D.B., 1995. Cordierite in felsic igneous rocks: a synthesis. Mineralogical Magazine 59, 311–325.

Clarke, D.B., Henry, A.S., White, M.A., 1998. Exploding xenoliths and the absence of "elephant" graveyards in granite batholiths. Journal of Structural Geology 20, 1325–1343.

Clemens, J.D., Wall, V.J., 1981. Origin and cristallization of some peraluminous (S-type) granitic magmas. Canadian Mineralogist 19, 111–131.

Clemens, J.D., Wall, V.J., 1984. Origin and evolution of a peraluminous silicic ignimbrite suite: the Violet Town Volcanics. Contributions to Mineralogy and Petrology 88, 354–371.

Cottin, J.Y., Lorand, J.P., Agrinier, P., Bodinier, J.L., Liégeois, J.P., 1998. Isotopic (O, Sr, Nd) and trace element geochemistry of the Laouni layered intrusions (Pan-African belt, Hoggar, Algeria): evidence for post-collisional continental tholeiitic magmas variably contaminated by continental crust. Lithos 45, 197–222.

Dahlquist, J.A., Rapela, C.W., Baldo, E.G., 2005. Petrogenesis of cordierite-bearing S-type granitoids in Sierra de Chepes, Famatinian orogen, Argentina. Journal of South American Earth Sciences 20, 231–251.

Debon, F., Lefort, P.L., 1988. A cationic classification of common plutonic rocks and their magmatic associations: principle, method, application. Bulletin de Minéralogie 111, 5.

Derridj, A., Ouzegane, K., Kienast, J.R., Belhai, D., 2003. P–T–X evolution in garnet pyroxenites from Tin Begane (Central Hoggar, Algeria). Journal of African Earth Science 37, 257–268.

Djouadi, M.T., Ferré, E., Gleizes, G., Caby, R., Lesquer, A., Bouchez, J.L., 1997. Oblique magmatic structures of two epizonal granite plutons, Hoggar, Algeria: late orogenic emplacement of transcurrent orogen. Tectonophysics 279, 350–374.

Duchesne, J.C., Berza, T., Liégeois, J.P., Vander Auwera, J., 1998. Shoshonitic liquid line of descent from diorite to granite: the Late Precambrian post-collisional Tismana pluton (South Carpathians, Romania). Lithos 45, 281–303.

Dupraz, J., Didier, J., 1988. Le complexe anatectique du Velay (massif central français): structure d'ensemble et évolution géologique. Géologie de la France 4, 73–88.

Féménias, O., Mercier, J.C., Nkono, C., Diot, H., Berza, T., tatu, M., Demaiffe, D., 2006. Calcic amphibole growth and compositions in calc-alkaline magmas: evidence from the Motru dyke swarm (Southern Carpathians, Romania). American Mineralogist 91, 73–81.

Fezaa, N., Liégeois, J.P., Abdallah, N., Ouabadi, A., 2005. Les massifs granitiques pan-africains du terrane d'In Ouzzal (Hoggar, Algérie), marqueurs de l'évolution métacratonique d'un vieux socle archéen: géochronologie et géochimie. Séminaire de géologie et de métallogénie des massifs du Hoggar et des Eglab. Tamanrasset, Algérie.

Flood, R.H., Shaw, S.E., 1975. A cordierite bearing granite suite from the New England batholith, NSW Austria. Contributions to Mineralogy and Petrology 52, 157–164.

Fourcade, S., Capevila, R., Ouabadi, A., Martineau, F., 2001. The origin and geodynamic significance of the Alpine cordierite-bearing granitoids of northern Algeria: a combined, petrological, mineralogical, geochemical and isotopic (O, H, Sr, Nd) study. Lithos 57, 187–216.

Gordillo, C.E., 1979. Observaciones sobre la petrologia de las rocascordieriticas de la Sierra de Cordoba. Boletin de la Academia Nacional de Ciencias, Cordoba, Argentina 53, 3–44.

Grant, J.A., 1985. Phase equilibria in partial melting of pelitic rocks. In: Ashworth, J.R. (Ed.), Migmatites. Blackie, Glasgow, pp. 86–144.

Guidotti, C.V., 1984. Micas in metamorphic rocks. In: Bailey, S.W. (Ed.) Micas. Mineralogical Society of America. Reviews in Mineralogy 13, 357–467.

Guillot, S., Le Fort, P., Pêcher, A., Roy Barman, M., Aprahamian, J., 1995. Contact metamorphism and depth of emplacement of the Manaslu granite (Central Nepal). Implications for Himalayan orogenesis. Tectonophysics 241, 99–119.

Guiraud, M., Powell, R., Cottin, J.-Y., 1996. Hydration of orthopyroxenes–cordierite-bearing assemblage at Laouni, Central Hoggar, Algeria. Journal of metamorphic Geology 14, 467–476.

Harley, S.L., Thompson, P., Hensen, B.J., Buick, S., 2002. Cordierite as a sensor of fluid conditions in high-grade metamorphism and crustal anatexis. Journal of Metamorphic Geology 20, 99–118.

Hollister, L.S., Grissom, G.C., Peters, E.K., Stowell, H.H., Sisson, V.B., 1987. Confirmation of the empirical correlation of Al in hornblende with pressure of solidification of calc-alkaline plutons. American Mineralogist 72, 231–239.

Jung, S., Hoernes, S., Mezger, K., 2000. Geochronology and petrogenesis of Pan-African, syn-tectonic, S-type and post-tectonic A-type granite (Namibia): products of melting of crustal sources, fractional crystallization and wall rock entrainment. Lithos 50, 259–287.

Kamineni, D.C., 1975. Chemical Mineralogy of some Cordierite-bearing Rocks near Yellowknife, Northwest Territiries, Canada. Contributions to Mineralogy and Petrology 53, 293–310.

Leake, B.E., Woolley, A.R., Arps, C.E.S., Birch, W.D., Gilbert, M.C., Grice, J.D., Hawthorne, F.C., Kato, A., Kisch, H.J., Krivovichev, V.G., Linthout, K., Laird, J., Mandarino, J.A., Maresch, W.V., Nickel, E.H., Rock, N.M.S., Schumacher, J.C., Smith, D.C., Stephenson, N.C.N., Ungaretti, L., Whittaker, E.J.W., Youzhi, G., 1997. Nomenclature of amphiboles: report of the Subcommittee on amphiboles of the International Mineralogical Association, Commission on new minerals and mineral Names. American Mineralogist 82, 1019–1037.

Le Breton, N., Thompson, A.B., 1988. Fluid-absent dehydratation melting of biotite in metamelites in the early stage of crustal anatexis. Contributions to Mineralogy and Petrology 99, 226–237.

Liégeois, J.P., Benhallou, A., Azzouni-Sekkal, A., Yahiaoui, R., Bonin, B., 2005. The Hoggar swell and volcanism: reactivation of the Precambrian Tuareg shield during Alpine convergence and West African Cenozoic volcanism. In: Foulger, G.R., Natland, J.H., Presnall, D.C., Anderson, D.L. (Eds.), Plates, Plumes and Paradigms, vol. 388. Geological Society of America, pp. 379–400 (Special Paper).

Liégeois, J.P., Black, R., 1987. Alkaline magmatism subsequent to collision in the Pan-African belt of the Adrar des Iforas. In: Fitton,

J.G., Upton, B.G.J. (Eds.), 2004, Alkaline Igneous Rocks, vol. 30. Geological Society of London, pp. 381–401 (Special Publication).

Liégeois, J.P., Black, R., Navez, J., Latouche, L., 1994. Early and late Pan-African orogenies in the Äir assembly of terranes (Tuareg shield, Niger). Precambrian Research 67, 59–88.

Liégeois, J.P., Diombana, D., Black, R., 1996. The Tessalit ring complex (Adrar des Iforas, Malian Tuareg shield): a Pan-African, post-collisional, syn-shear, alkaline granite intrusion. In: Petrology and Geochemistry of Magmatic Suites of Rocks in the Continental and Oceanic Crust, A Volume Dedicated to J. Michot, D. Demaiffe (Ed.), ULB-MRAC, Brussels, pp. 227–244.

Liégeois, J.P., Navez, J., Hertogen, J., Black, R., 1998. Contrasting origin of post-collisional high calc-alkaline and shoshonitic versus alkaline and peralkaline granitoids. The use of sliding normalisation. Lithos 45, 1–28.

Liégeois, J.P., Latouche, L., Boughrara, M., Navez, J., Guiraud, M., 2003. The LATEA metacraton (Central Hoggar, Tuareg shield, Algeria): behaviour of an old passive margin during the Pan-African orogeny. Journal of African Earth Science 37, 161–190.

Ludwig, K.R., 2001. Squid 1.02: A User's Manual, Berkeley Geochronology Center. Special Publication, 19pp.

Ludwig, K.R., 2003. User's manual for Isoplot/3, a geochronological toolkit for Microsoft Excel. Berkeley Geochronology Center, Special Publication, 14, 71pp.

Lugmair, G.W., Marti, K., 1978. Lunar initial $^{143}Nd/^{144}Nd$: differential evolution of the lunar crust and mantle. Earth and Planetary Science Letters 39, 349–357.

Mathias, M., 1952. An unusual cordierite-rock from Upington, Cape Province. South Africa Mineralogical Magazine 29, 936–945.

Moreau, C., Demaiffe, D., Bellion, Y., Boullier, A.M., 1994. A tectonic model for the location of Paleozoic ring-complexes in Aïr (Niger, West Africa). Tectonophysics 234, 129–146.

Morimoto, N., Fabries, J., Ferguson, A.K., Ginzburg, I.V., Ross, M., Seifeit, F.A., Zussman, J., 1989. Nomenclature of pyroxenes. Canadian Mineralogist 27, 143–156.

Nachit, H., Razafimahefa, N., Stussi, J.M., Caron, J., 1985. Composition chimique des biotites et typologie magmatique des granitoïdes. Comptes Rendus de l'Académie des Sciences, Paris 301, 813–818.

Nelson, D.R., 1997. Compilation of SHRIMP U–Pb zircon geochronology data. 1996. Geological Survey of Western Australia 2, 1–198.

Ouabadi, A., 1994. Pétrologie, géochimie et origine des granitoïdes hyperalumineux à cordiérite (Cap Bougaroun, Beni-Toufout et Filfila, Algerie nord-orientale). Thèse, Doctorat ès Sciences. U.S.T.H.B. 218pp.

Ouzegane, K., Bendaoud, A., Kienast, J.R., Touret, J.L.R., 2001. Pressure–temperature–fluid evolution in Eburnean metabasites and metapelites from Tamanrasset Hoggar, Algeria. Journal of Geology 109, 213–230.

Ouzegane, K., Kienast, J.R., Bendaoud, A., Drareni, A., 2003. A review of Archaean and Paleoproterozoic evolution of the In Ouzzal granulitic terrane (Western Hoggar, Algeria). Journal of African Earth Science 37, 207–227.

Paquette, J.L., Caby, R., Djouadi, M.T., Bouchez, J.L., 1998. U–Pb dating of the end of Pan-African orogeny in the Tuareg shield: the post-collisional syn-shear Tioueine pluton (western Hoggar, Algeria). Lithos 45, 245–253.

Pattison, D.R.M., Spear, F.S., Debuhr, C.L., Cheney, J.T., Guidotti, C.V., 1996. Thermodynamic modeling of the reaction muscovite + cordierite $\rightarrow Al_2SiO_5$ + biotite + quartz + H_2O: constraints from natural assemblages and implications for the metapelitic petrogenetic grid. Contributions to Mineralogy and Petrology 124, 82–89.

Peucat, J.J., Drareni, A., Latouche, L., Deloule, E., Vidal, P., 2003. U–Pb zircon (TIMS and SIMS) and Sm-Nd whole rock geochronology of the Gour Oumalelen granulitic basement, Hoggar massif, Tuareg shield, Algeria. Journal of African Earth Science 37, 229–239.

Pearce, J.A., 1982. Role of the Sub-continental Lithosphere in Magma Genesis at Active Continental Margins. Continental Basalts and Mantle Xenoliths. Shiva Publication, Cheshire, UK, pp. 230–249.

Pidgeon, R.T., Furfaro, D., Kennedy, A.K., Nemchin, A.A., Van Bronswijk, W., 1994. Calibration of zircon standards for the Curtin SHRIMP II. United States Geological Survey circular 1107, 251.

Rapela, C.W., Baldo, E.G., Pankhurst, R.J., Saavedra, J., 2002. Cordieritite and Leucogranite Formation during Emplacement of Highly Peraluminous Magma: the El Pilon Granite Complex (Sierras Pampeanas, Argentina). Journal of Petrology 43, 1003–1028.

Rickwood, P.C., 1989. Boundary lines within petrologic diagrams which use oxides of major and minor elements. Lithos 22, 247–264.

Schmidt, M.W., 1992. Amphibole composition in tonalite as a function of pressure: an experimental calibration of Al in hornblende barometer. Contributions to Mineralogy and Petrology 110, 304–310.

Schreyer, W., Gordillo, C.E., Werding, G., 1979. A new sodian beryllian cordierite from Soto, Argentina, and the relationship between distorsion index, Be content and state of hydratation. Contributions to Mineralogy and Petrology 70, 421–428.

Skippen, G.B., Gunter, A.E., 1996. The thermodynamic properties of H_2O in magnesium and iron cordierite. Contributions to Mineralogy and Petrology 14, 467–476.

Stacey, J.S., Kramers, J.D., 1975. Approximation of terrestrial lead isotopic evolution by a two-stage model. Earth and Planetary Science Letters 26, 207–221.

Steiger, R.H., Jäger, E., 1977. Subcommission on geochronology: convention on the use of decay constants in geo- and cosmochronology. Earth and Planetary Sciences Letters 36, 359–362.

Streckeisen, A., Le Maitre, R.W.L., 1979. A chemical approximation to the modal QAPF Classification of the igneous rocks. Neues Yahrbuch Mineralogie. Abhver 136, 169–206.

Sun, S.S., 1980. Lead isotopic study of young volcanic rocks from mid-ocean ridges, ocean islands and islands arcs. Philosophical Transactions of the Royal Society of London A297, 409–445.

Sylvester, P.J., 1998. Post-collisional strongly peraluminous granites. Lithos 45, 29–44.

Taylor, S.R., McLennan, S.M., 1980. The composition and evolution of the continental crust: rare earth element. Evidence from sedimentary rocks. Philosophical Transfer Royal Society of London 301, 381–389.

Thompson, A.B., 1976. Mineral reactions in pelitic rocks. American Journal Society 276, 401–414.

Ugidos, J.M., 1988. New aspects and considerations on the assimilation of cordierite-bearing rocks. Revista de la Societad Geologica de Espana 1, 129–133.

Vielzeuf, D., Holloway, J.R., 1988. Experimental determination of the fluid-absent melting relations in the pelitic system. Consequences for crustal differentiation. Contributions to Mineralogy and Petrology 98, 257–276.

Vielzeuf, D., Montel, J.M., 1994. Partial melting of metagreywackes. Part I. Fluid-absent experiments and phase relationships. Contributions to Mineralogy and Petrology 117, 375–393.

Watson, E.B., Harrison, T.M., 1983. Zircon saturation revisited: temperature and composition effects in a variety of crustal magma types. Earth and Planetary Science Letters 64, 295–304.

Zetoutou, S., Ouzegane, K., Boubazine, S., Kienast, J.R., 2004. Azrou N'Fad (Central Hoggar, Algeria) one of the deepest terranes of Latea: arguments based on P–T evolution in eclogite. Journal of African Earth Science 39, 193–200.